Stem Cell Reports
Article

ISSCR

OPEN ACCESS

Real-Time Monitoring of Glutathione in Living Cells Reveals that High Glutathione Levels Are Required to Maintain Stem Cell Function

Eui Man Jeong,[1,2] Ji-Hye Yoon,[3] Jisun Lim,[1,4] Ji-Woong Shin,[1] A. Young Cho,[3] Jinbeom Heo,[4] Ki Baek Lee,[1] Jin-Haeng Lee,[1] Won Jong Lee,[1] Hyo-Jun Kim,[1] Young Hoon Son,[1] Seok-Jin Lee,[1] Sung-Yup Cho,[1] Dong-Myung Shin,[4,*] Kihang Choi,[3,*] and In-Gyu Kim[1,2,*]

[1]Department of Biochemistry and Molecular Biology, Seoul National University College of Medicine, Seoul 03080, Republic of Korea
[2]Institute of Human-Environment Interface Biology, Seoul National University College of Medicine, Seoul 03080, Republic of Korea
[3]Department of Chemistry, Korea University, Seoul 02841, Republic of Korea
[4]Department of Biomedical Sciences, University of Ulsan College of Medicine, Seoul 05505, Republic of Korea
*Correspondence: d0shin03@amc.seoul.kr (D.-M.S.), kchoi@korea.ac.kr (K.C.), igkim@plaza.snu.ac.kr (I.-G.K.)
https://doi.org/10.1016/j.stemcr.2017.12.007

SUMMARY

The core functions of stem cells (SCs) are critically regulated by their cellular redox status. Glutathione is the most abundant non-protein thiol functioning as an antioxidant and a redox regulator. However, an investigation into the relationship between glutathione-mediated redox capacity and SC activities is hindered by lack of probe. Here, we demonstrate that cyanoacrylamide-based coumarin derivatives are ratiometric probes suitable for the real-time monitoring of glutathione levels in living SCs. These probes revealed that glutathione levels are heterogeneous among subcellular organelles and among individual cells and show dynamic changes and heterogeneity in repopulating SCs depending on oxidative stress or culture conditions. Importantly, a subpopulation of SCs with high glutathione levels exhibited increased stemness and migration activities *in vitro* and showed improved therapeutic efficiency in treating asthma. Our results indicate that high glutathione levels are required for maintaining SC functions, and monitoring glutathione dynamics and heterogeneity can advance our understanding of the cellular responses to oxidative stress.

INTRODUCTION

Reactive oxygen species (ROS) are important signaling molecules that regulate cellular metabolism, proliferation, and survival (Winterbourn and Hampton, 2008). An increase of ROS induces the thiol oxidation of cysteine residues on signaling proteins, resulting in alterations of protein activities to regulate cellular functions. In particular, ROS-mediated oxidation plays an important role in regulating a variety of signaling proteins in stem cells (SCs) that influence self-renewal capacity, pluripotency, viability, and genomic stability, including OCT4, NRF2, FoxOs, APE1/Ref-1, ATM, HIF-1, p38, and p53 (Wang et al., 2013). For example, OCT4, a pluripotency-related transcription factor, is inactivated via cysteine oxidation under glutamine-depleted conditions, favoring the differentiation and functional maturation of embryonic SCs (ESCs) (Marsboom et al., 2016). Disruption of *Nrf2*, a master regulator of redox homeostasis, impinges upon the functions of embryonic and adult SCs such as the self-renewal and pluripotency in ESCs (Jang et al., 2014), the migration and retention of hematopoietic SCs in the bone marrow niche (Tsai et al., 2013), and the proliferation and homeostasis in intestinal (Hochmuth et al., 2011) and airway basal SCs (Paul et al., 2014). Thus, the cellular redox regulation is critical for maintaining stemness and functional potency of ESCs and adult SCs.

Cellular redox homeostasis depends on the balance between ROS production and their elimination via enzymes and antioxidant molecules such as glutathione (GSH), a thiol-containing tripeptide that plays a major role in maintaining redox homeostasis owing to its high concentration (approximately 1–10 mM). GSH is synthesized in the cytosol and is then transported to cellular compartments such as the mitochondria, nucleus, and ER, where redox buffering is required for organelle-specific functions. GSH eliminates hydrogen peroxide (H_2O_2) through a glutathione peroxidase-catalyzed reaction, producing water and oxidized GSH (GSSG), which is regenerated to GSH by glutathione reductase at the expense of NADPH (Lu, 2013). Therefore, changes in the GSH levels in response to oxidative stress can reflect the redox buffering capacity of a particular cell type or cellular compartment. Moreover, GSH also acts as a regulator for ROS-triggered signal transmission. GSH reduces ROS-induced disulfides in signaling proteins, either by glutaredoxin or by forming *S*-glutathionylated proteins through a thiol-disulfide exchange reaction, thereby modulating the intensity and duration of redox signaling (Winterbourn and Hampton, 2008). Furthermore, ESCs and inducible pluripotent SCs harbor particularly high GSH levels, which confer protection against unfavorable DNA damage (Dannenmann et al., 2015). Thus, monitoring the dynamic changes of GSH levels in living SCs is required to evaluate the redox buffering capacity and signaling processes that modulate SC functions during several physiological and pathological processes. However, obtaining a detailed understanding of the GSH-based redox system has thus far been limited owing to the lack of direct and reliable tools.

Various techniques have been used to estimate GSH levels in living cells to date, including redox-sensitive fluorescent proteins such as rxYFP and roGFP (Gutscher et al., 2008). Since the thiol-disulfide status of these fluorescent proteins is in equilibrium with that of cellular GSH, this method can provide information on the GSH/GSSG redox potential but cannot directly monitor the changes in GSH levels. In addition, the poor efficiency of transfection and consequent cellular damage hinder the application of this genetic method for a wide range of cell types. Several thiol-reactive fluorescent chemical dyes have also been developed as GSH sensors to overcome these problems (Yin et al., 2013). However, these dyes still have drawbacks such as irreversibility, slow kinetics (Kim et al., 2011), low fluorescence quantum yields (Chen et al., 2015), or limited subcellular localization (Umezawa et al., 2017). Moreover, previous works on GSH monitoring have not paid enough attention to the possible errors caused by reactive thiols in cellular proteins.

To overcome the limitations of current GSH probes, we previously reported the synthesis of a coumarin derivative bearing a conjugated 2-cyanoacrylamide group, designated FreSHtracer (fluorescent real-time thiol tracer; Figure 1A), which reacts reversibly with thiols in aqueous solutions (Cho and Choi, 2012). The present study showed that FreSHtracer is a powerful tool for real-time monitoring of GSH dynamics and heterogeneity in living SCs, and revealed that SCs cultured under conventional conditions exhibit the downregulation of GSH levels that results in deterioration of self-renewal and migration function. Therefore, our results prove that monitoring glutathione contents and dynamics in living SCs can be used as a marker to evaluate SC function and enhance its therapeutic potency.

RESULTS

FreSHtracer Is a Ratiometric Probe Suitable for Measuring and Monitoring GSH Levels

We first investigated whether FreSHtracer could be suitable for measuring and monitoring GSH levels even in the presence of abundant cellular protein thiols. In the reaction with GSH, FreSHtracer showed a spectral shift of the λ_{max} of its ultraviolet-visible absorption from 520 nm to 430 nm, resulting in decreased fluorescence emission intensity at 580 nm (F_{580}, λ_{ex} 520 nm) and increased fluorescence intensity at 510 nm (F_{510}, λ_{ex} 430 nm; Figures 1A and S1A). The apparent dissociation constant (K_D) value for GSH was estimated at 3.6 mM and was unaffected by pH changes ranging from 6.0 to 9.0 (Table S1 and Figure S1B). Notably, the F_{510}/F_{580} ratio (FR) correlated with the GSH concentration (R^2 = 0.9938; Figure 1B), indicating that FreSHtracer can ratiometrically report the GSH concentration. When GSH was added to FreSHtracer, the FR rapidly increased, reaching a plateau within 5 min (Figure 1C), and was then stoichiometrically decreased by treatment with the thiol-specific oxidants diamide and *N*-ethylmaleimide (NEM), as well as with H_2O_2 treatment in a dose-dependent manner (Figures 1C, 1D, and S1C–S1E), demonstrating a reversible reaction with GSH. Moreover, the FR was unchanged by treatment with GSSG and only increased when both glutathione reductase and NADPH were added to the mixture to reduce GSSG to GSH (Figure 1E), indicating the specific reaction of FreSHtracer with GSH.

We next characterized the reaction between FreSHtracer and accessible cysteine thiols in cellular proteins (PSH), which were estimated at a concentration of 1.95 ± 0.11 mM in 25 mg/mL protein of the HeLa cell lysates using Ellman's assay, comprising up to 70% of the total cellular thiols (Hansen et al., 2009). When added to diluted protein solutions, the FR slowly increased, reaching a plateau after 90 min (Figure 1F) in a protein concentration-dependent manner, but remained constant in concentrated protein solutions (Figure 1G). These results were confirmed by calculation of the rate constants, showing that the reaction with PSH was approximately 12-fold slower than that with GSH (Figure S1F). The FR of protein solutions decreased by treatment with diamide, but not with H_2O_2, indicating that PSH is oxidized by diamide but resistant to H_2O_2-induced oxidation (Figures 1H and S1G). When the changes in the FR of FreSHtracer were monitored in protein solutions spiked with various concentrations of GSH, the FR was found to increase rapidly within 5 min and then gradually increased further over a period of 1.5 hr (Figures 1I and S1H), showing the combined kinetics for GSH and PSH. Moreover, when plotted against the GSH concentration, the FR was shown to increase in a GSH-concentration-dependent manner (Figure 1J). Although the FR was affected by the cellular proteins added, this dependency on the protein concentration became less significant at higher concentration ranges (Figure S1I). Therefore, the FR is expected to be mainly dependent on the GSH concentration and not significantly affected by typical protein concentration variations (50–200 mg/mL) in intact cells (Finka and Goloubinoff, 2013). Considering that the PSH-induced FR remained constant, these results imply that the total FR could be divided into GSH- and PSH-dependent FR values (FR_{GSH} and FR_{PSH}, respectively). Consistently, treatment with H_2O_2 diminished only the FR_{GSH} with no effect on the FR_{PSH}, whereas treatment with diamide resulted in a dose-dependent decrease in both FR_{PSH} and FR_{GSH} (Figures 1K and S1G). Thus, these results demonstrate that FreSHtracer is capable of monitoring the ROS-induced GSH changes in a cell homogenate.

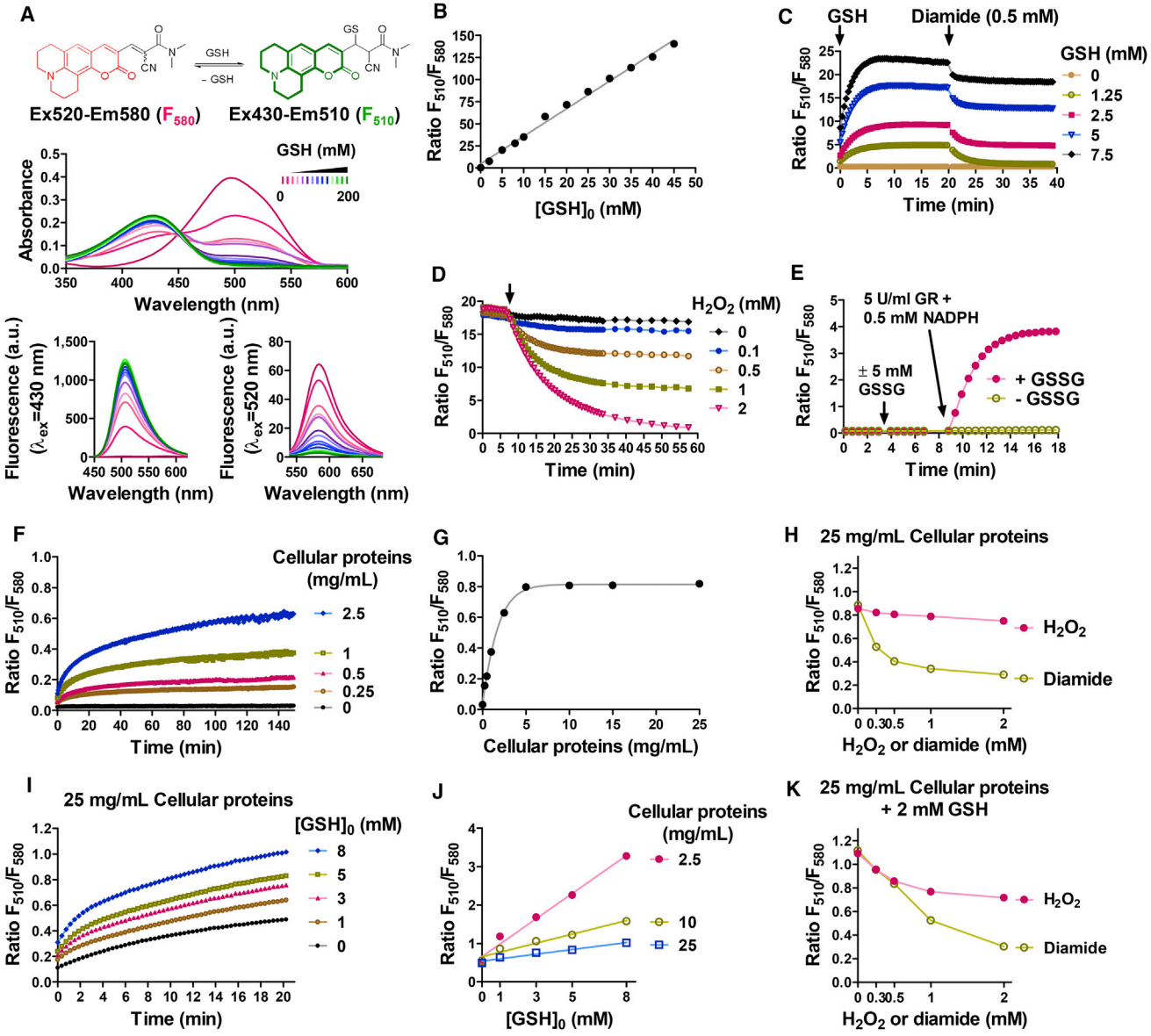

Figure 1. FreSHtracer Is a Reversible and Ratiometric Probe for Glutathione

(A) Changes in the absorption and fluorescence spectra of FreSHtracer when reacted with increasing concentrations of glutathione (GSH).

(B) Fluorescence ratio (F_{510}/F_{580}; FR) of FreSHtracer plotted as a function of the GSH concentration.

(C) Reversible reaction of FreSHtracer with GSH following treatment with diamide.

(D and E) GSH-specific reaction of FreSHtracer. FreSHtracer equilibrated with GSH (5 mM; 15 min) was treated with H_2O_2 (0–2 mM) (D), and FreSHtracer equilibrated with oxidized GSH (GSSG, 5 mM) was treated with GSH reductase (5 U/mL) and 0.5 mM NADPH (E).

(F and G) Fluorescence properties of FreSHtracer in dialyzed cell lysates. The FR change was monitored in dialyzed HeLa cell lysates (F) and then plotted against the protein concentration (G).

(H) Effect of oxidants on the PSH-induced FR. Dialyzed cell lysates (25 mg/mL protein) were incubated with FreSHtracer (2 hr) and treated with diamide or H_2O_2 for 1 hr.

(I and J) Fluorescence properties of FreSHtracer in PSH-GSH mixtures. FreSHtracer was added to dialyzed cell lysates (25 mg/mL protein) spiked with various GSH concentrations. The FR change was monitored for 20 min (I). The final FR value was plotted against the GSH concentration (J).

(K) Effect of oxidants on the FR of the PSH-GSH mixture. PSH-GSH mixtures (25 mg/mL protein and 2 mM GSH) were incubated with FreSHtracer (2 hr) and treated with diamide or H_2O_2 for 1 hr.

See also Figure S1.

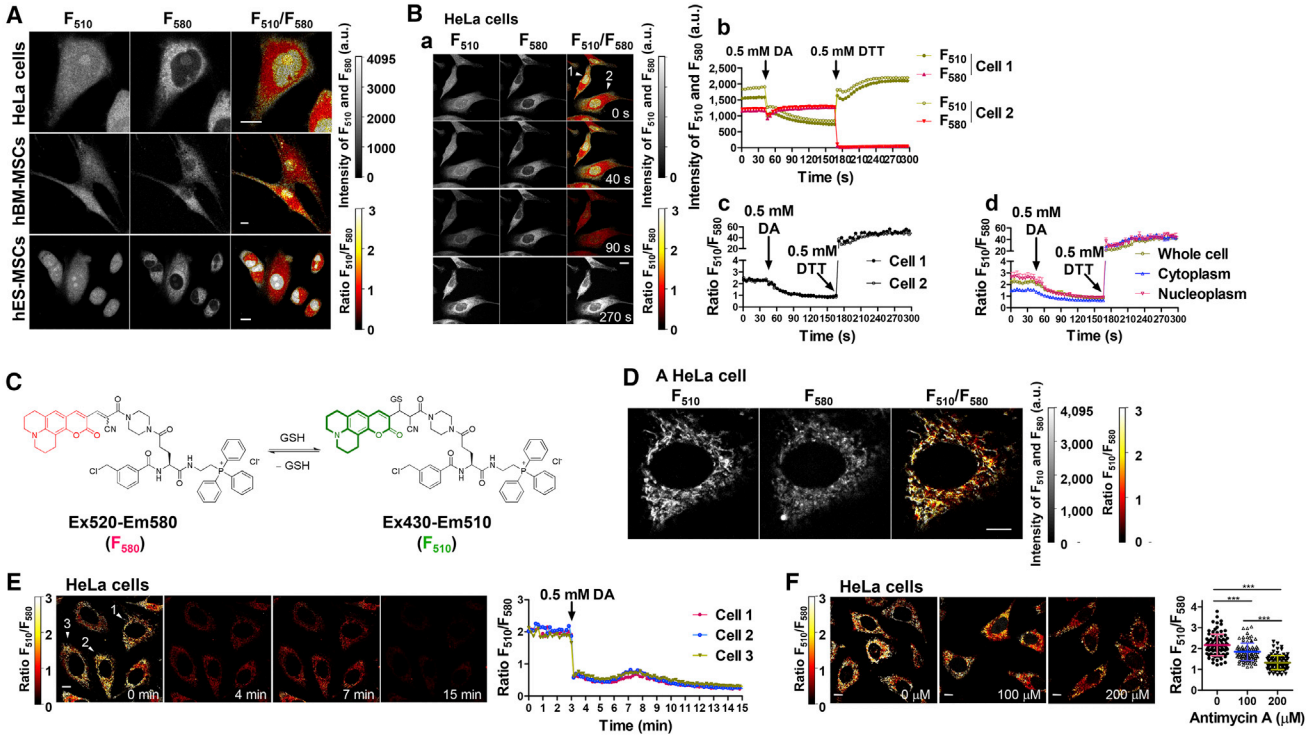

Figure 2. FreSHtracer Visualizes GSH Levels within Subcellular Compartments in Living Cells

(A) Representative confocal images of F_{510} and F_{580}, and pseudo-color images of the fluorescence ratio (FR) for HeLa cells, hBM-MSCs, and hES-MSCs. The cells were incubated with FreSHtracer (5 μM) for 2 hr. Images of a HeLa cell and hBM-MSCs are the same, with cells indicated by arrows in Figure 4A (0 min).

(B) A reversible reaction of FreSHtracer with intracellular thiols. In HeLa cells equilibrated FreSHtracer (5 μM, 2 hr), F_{510} and F_{580} were monitored at 5-s intervals after treatment with diamide (DA), followed by 0.5 mM DTT. (a) Confocal and pseudo-color images of FreSHtracer-loaded cells indicated by numbered arrowheads. (b and c) The F_{510}, F_{580}, and FR of the two cells (arrowheads) were monitored. (d) The average FR values in the whole cell, cytoplasm, and nucleoplasm (n = 4 cells/time point) are shown.

(C) The structure of MitoFreSHtracer, and changes in its fluorescence spectra when reacted with GSH.

(D) Confocal and ratiometric pseudo-color images of a MitoFreSHtracer-loaded (10 μM, 1.5 hr) HeLa cell.

Images are the same with the cell indicated by arrowhead 1 in E (0 min).

(E) Effect of DA (0.5 mM) on the FR within MitoFreSHtracer-loaded HeLa cells. Left: pseudo-color images of the FR. Right: time course of FR changes within the indicated cells (arrowheads).

(F) Effect of antimycin A (0, 100, 200 μM; 75 min) on FR values in MitoFreSHtracer-loaded HeLa cells. Left: pseudo-color images of the FR. Right: concentration-dependent decreases in the FR values within antimycin A-treated cells (n = 90 cells from n = 3 independent experiments).

Data represent the mean ± SEM of the FR; ***p < 0.001. Scale bars, 10 μm (A, B, D, E, F). See also Figures S2–S4.

GSH Levels Are Heterogeneous in the Subcellular Organelles of Living Cells

Next, to utilize FreSHtracer for GSH monitoring in living cells, we evaluated its cytotoxicity. Treatment of up to 10 μM FreSHtracer for 24 hr showed no effect on the viability of HeLa cells and human mesenchymal SCs derived from bone marrow (hBM-MSCs) and ESCs (hES-MSCs) (Hong et al., 2015) (Figure S2). HeLa cells were equilibrated with treatment of 5 μM FreSHtracer for 2 hr. Confocal and ratiometric pseudo-color images revealed that FreSHtracer was distributed inside the cells, exhibiting a wide range of FR values (Figure 2A). The FR in the nucleus was about 1.5- to 2-fold higher than that of the cytoplasm. The FR of the nucleolus revealed relatively lower GSH levels, and the FR of the peripheral cytoplasm was higher than that of other regions. Moreover, variable FR values were observed in the cytoplasm, which produced a mosaic pattern in the pseudo-color images, possibly arising from GSH in the ER and mitochondria. When HeLa cells were treated with diamide following equilibration with 5 μM FreSHtracer for 2 hr, the FR gradually decreased by diamide (or NEM) and then rapidly increased by DTT (Figures 2B and S3), demonstrating that FreSHtracer reacts reversibly with thiols in the intracellular environment.

The mitochondrion is the major site of endogenous ROS generation during normal oxidative metabolism (Balaban et al., 2005). Cytosolic GSH is transported to the mitochondria, preventing macromolecular damage and modulating ROS-induced signaling (Mari et al., 2013). To further analyze the FR heterogeneity in the cytoplasm, we synthesized a mitochondria-targeting FreSHtracer derivative, designated MitoFreSHtracer (Figure 2C), by attaching a triphenylphosphonium moiety to FreSHtracer (Murphy and Smith, 2007). MitoFreSHtracer reacted rapidly and reversibly with GSH, exhibited GSH-dependent FR values similar to those of FreSHtracer (K_D = 1.3 mM, Figures S4A–S4C), and showed no cytotoxic effect on HeLa cells with treatment up to 10 μM for 24 hr (Figure S4D).

Confocal images revealed that MitoFreSHtracer localized to the mitochondria in HeLa cells (Figure 2D), and the FR decreased upon diamide treatment (Figure 2E), indicating that GSH levels within the mitochondria can be monitored by MitoFreSHtracer. Remarkably, there was wide variation in the FR values among mitochondria within a single cell, even under normal culture conditions (Figure 2D), indicating that the GSH levels in the mitochondria of a single cell are heterogeneous. Moreover, a concentration-dependent decrease in the FR was observed when the cells were treated with antimycin A, which generates ROS in mitochondria by inhibiting electron transport (Drose and Brandt, 2008) (Figure 2F). Simultaneous analyses showed that mitochondrial ROS levels increased with treatment of DHR123, a non-fluorescent rhodamine derivative that localizes to the mitochondria and emits fluorescence when oxidized by ROS (Figures S4E and S4F). Taken together, these results demonstrate that GSH levels differ among organelles as well as among different regions within the same compartment of a live cell.

Real-Time Measurement of GSH Concentrations in Living Cells

Although GSH is the most abundant thiol in cells, proteins constitute a significant portion of cellular thiol (Hansen et al., 2009). Thus, we examined whether FreSHtracer could be not significantly affected by the presence of protein thiols for reporting the continuous changes of GSH levels in living cells. When HeLa cells were treated with various concentrations of buthionine sulfoximine (BSO) for 48 hr to suppress GSH synthesis, measurements of the FR in the GSH-depleted cells showed that the FR_{GSH} accounted for approximately 55% of the total FR in normal cells, and the intracellular GSH concentration, which was independently measured by luminescence-based assays in cell lysates, was directly correlated with the FR determined by confocal microscopy (R^2 = 0.9135; Figure 3A) and flow cytometry (R^2 = 0.9753; Figure 3B).

The *in vitro* experiments described above established that H_2O_2 treatment diminishes only the FR_{GSH}, while having little effect on the FR_{PSH} (Figures 1H and 1K). In line with these *in vitro* data, the GSH-depleted cells showed no change in their FR values following the addition of either 100 μM or 500 μM H_2O_2 over a period of 40 min (Figure 3C), indicating that oxidation of GSH, and not PSH, caused the FR change in H_2O_2-treated cells. Thus, FreSHtracer can report the real-time dynamic changes of GSH concentration in live cells under oxidative stress. Interestingly, when the GSH-depleted cells were treated with diamide as a control experiment, the FR decreased but was then immediately restored to the original level (Figure 3D). This restoring activity was abrogated by treatment with 1-chloro-2,4-dinitrobenzene, an inhibitor of thioredoxin reductase (Figure 3E), indicating that thioredoxin, instead of GSH, is required to reduce the disulfides of PSH. These results indicate that FreSHtracer can successfully distinguish between GSH and PSH in living cells.

Cellular GSH Levels Dynamically Change under Oxidative Stress

ROS production by various cellular conditions significantly affected SC functions such as self-renewal and differentiation (Ito and Suda, 2014). Thus, we monitored the H_2O_2-induced changes in GSH levels. When HeLa cells and hBM-MSCs were treated with H_2O_2, the FR decreased rapidly, then remained unchanged before increasing slowly, and ultimately returned to the untreated level. The profile and time course of FR changes in the cytoplasm and nucleoplasm were similar to those observed in whole cells (Figure 4A). Notably, GSH levels in HeLa cells were more sensitive to H_2O_2 treatment than those in hBM-MSCs. In HeLa cells treated with increasing concentrations of H_2O_2, both the decrease in the FR and the lag time for recovery were accentuated (Figure 4B).

To confirm these results, we monitored the GSH changes induced by endogenously produced ROS. In macrophages, ROS are produced by NADPH oxidase when the cells are activated. Therefore, RAW264.7 cells were loaded with FreSHtracer and treated with phorbol 12-myristate 13-acetate (PMA). Confocal microscopy revealed that the FR decreased gradually over 30 min upon PMA treatment in every region of the treated cells and was then slowly restored to the control level during the following 30 min (Figure 4C). Moreover, ROS production was also reported to increase in cells cultured at a low density or in serum-deprived medium (Gutscher et al., 2008). Therefore, we monitored the effect of culture conditions on the changes of GSH levels. Exposure of HeLa cells to serum-free medium for 18 hr significantly reduced the FR in the cytoplasm and in the nucleoplasm (Figure 4D). When cultured at different

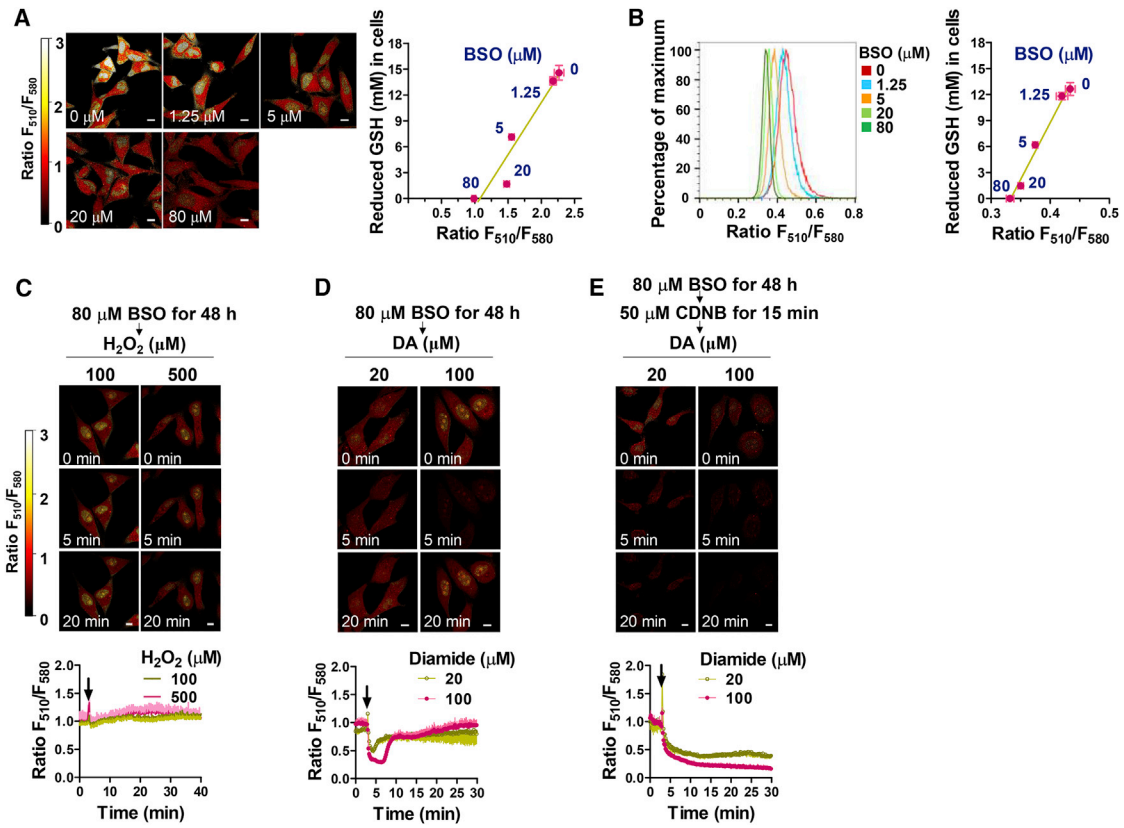

Figure 3. FreSHtracer Can Report the GSH Concentration within Live Cells

(A and B) Determination of the F_{510}/F_{580} ratio (FR) fraction attributable to GSH (FR_{GSH}). The FR within buthionine sulfoximine (BSO)-treated HeLa cells (3–4 × 10^3 cells/cm^2; 48 hr) in confocal imaging of each cell (n = 10 cells; A) or the FR within flow-cytometric analysis of BSO-treated cells (n = 3 independent biological replicates; B) were plotted against the GSH concentration determined by luminescence-based methods following cell lysis (n = 3 independent biological replicates; A and B, right).

(C–E) Effect of oxidants on the FR of GSH-depleted cells (FR_{PSH}). BSO-treated HeLa cells (48 hr, 80 μM), equilibrated with FreSHtracer (2 hr, 5 μM), were treated for 15 min with (E) or without (C and D) 50 μM 1-chloro-2,4-dinitrobenzene (CDNB), an irreversible inhibitor of thioredoxin reductase. Fluorescence intensities were measured every 10 s by confocal microscopy following treatment with H_2O_2 (C) or diamide (DA; D and E). Ratiometric pseudo-color images (C–E, upper) depict the FR (n = 4 cells/time point; C–E, lower). Arrows indicate time points of treatment of H_2O_2 or diamide.

All error bars represent mean ± SEM. Scale bars, 10 μm (A, C, D, E).

densities, the average FR of densely cultured HeLa cells was significantly higher than that of sparsely cultured cells, despite the large variation in the FR, particularly in the nucleoplasm (Figure 4E).

We then extended these results to monitor the GSH levels in hBM-MSCs. The cells were serially subcultured at different seeding densities. Flow-cytometric analysis showed that the hBM-MSC populations were heterogeneous with respect to GSH levels, and, notably, the number of cells with a high GSH content (GSH^{High}) gradually decreased with increasing passages, especially when cultured at a low cell density (Figure 4F), indicating that GSH levels in SCs depend on the culture conditions. Together, these results demonstrate that GSH levels are dynamically changed in response to oxidative stress, and that FreSHtracer can provide spatiotemporal information of GSH levels for estimating the redox buffering capacity of individual cells.

High GSH Levels Are Required for Stem Cell Function

To further explore the biological significance of the reprogrammed GSH levels in SCs, we sorted hBM-MSCs by flow cytometry and divided them into three subpopulations based on the FR (FR^{High}, FR^{Mid}, and FR^{Low} cells; Figure S5A), following the rapid removal of FreSHtracer in sorted cells (Figure S5B). When we compared the functional characteristics of sorted SC subpopulations *in vitro*, the FR^{High} hBM-MSCs, compared with FR^{Mid} and FR^{Low} cells, significantly enhanced the cellular functions regarding colony-forming unit fibroblasts (CFU-F) and

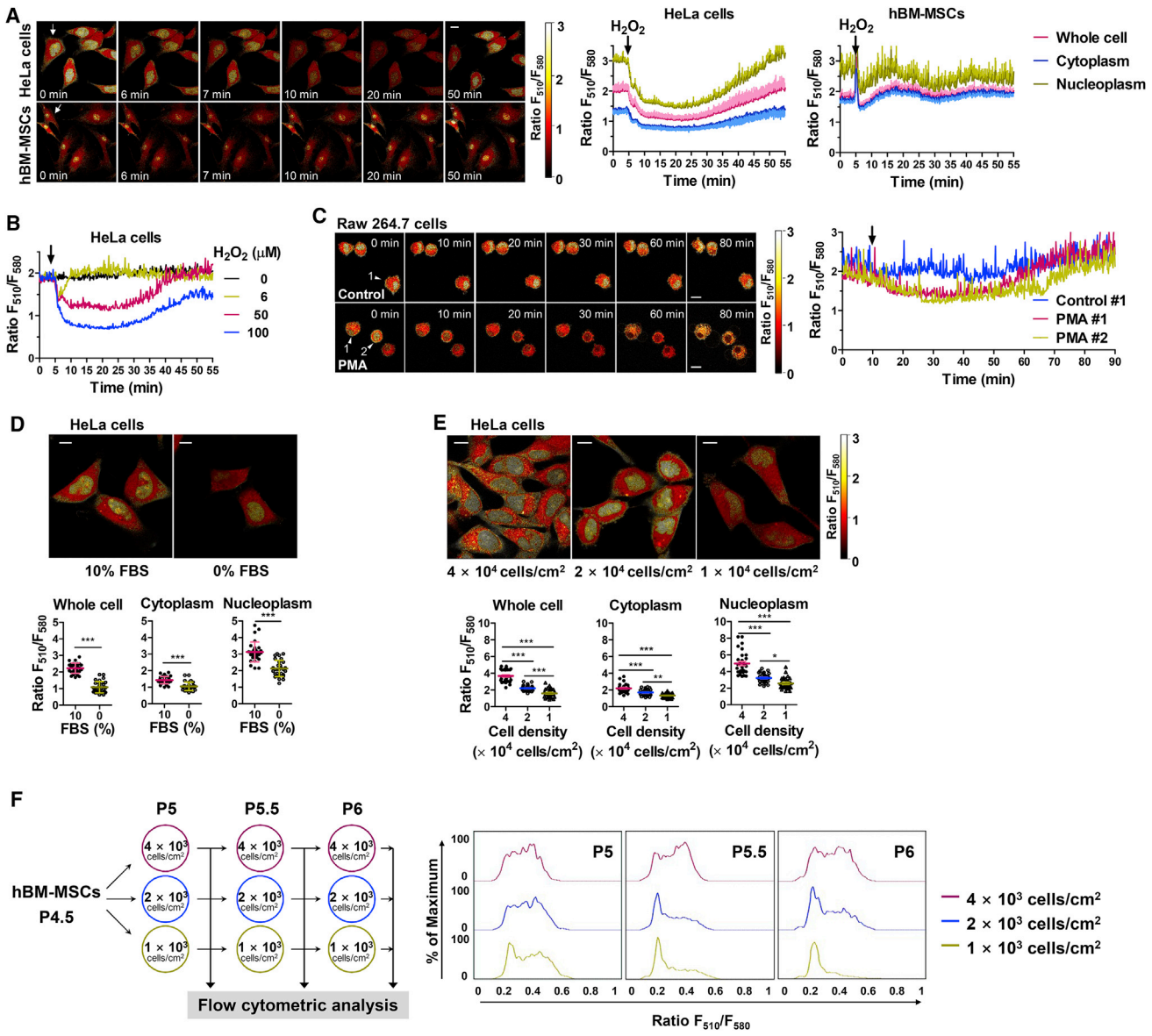

Figure 4. Heterogeneity and Dynamic Changes of GSH Levels in Living Cells

(A and B) HeLa cells and hBM-MSCs were incubated with FreSHtracer (5 μM) for 2 hr, and the fluorescence ratio (FR) changes in response to H_2O_2 treatment were monitored. HeLa cells and hBM-MSCs equilibrated with FreSHtracer (5 μM, 2 hr) were treated with 50 μM and 100 μM H_2O_2, respectively, and images were recorded every 10 s using a confocal microscope. Ratiometric pseudo-color images of cells (A, left) depicting the FR of whole cells, the cytoplasm, and the nucleoplasm (n = 7 cells/time point in HeLa cells; n = 20 cells/time point in hBM-MSCs; A, right), and the H_2O_2 concentration-dependent changes of FR in HeLa cells (B) are shown. A HeLa cell and hBM-MSCs images (A, left) indicated by arrows are reused in Figure 2A.

(C) FR changes of RAW264.7 cells following phorbol 12-myristate 13-acetate (PMA) treatment. RAW264.7 cells equilibrated with FreSHtracer (4 hr, 5 μM) were treated with either ethanol (control) or PMA (0.5 μg/mL). Images were taken every 10 s using a confocal microscope. Left: ratiometric pseudo-color images of control and PMA-treated RAW264.7 cells. Right: FR changes following PMA treatment within the indicated cells (arrowheads).

(D) Effect of serum deprivation on the FR. Following equilibration for 2 hr with 5 μM FreSHtracer, images were taken using a confocal microscope. Upper panel: pseudo-color images depicting the FR. Lower panel: FR within whole cells, the cytoplasm, and the nucleoplasm (n = 30 cells from n = 3 independent experiments).

(legend continued on next page)

the chemoattraction to platelet-derived growth factor (PDGF) (Figures S5C and S5D).

To further validate the improved functionality of SCs with a high GSH content, via fluorescence-activated cell sorting we sorted hES-MSCs into FR^{High}, FR^{Mid}, and FR^{Low} subpopulations based on the FR (Figure 5A). The GSH concentrations in the cell lysates from each population were directly proportional to their FR levels, validating the FR-based sorting method (Figure 5B). Intriguingly, the decrease of FR and the lag time for recovery following treatment with 100 μM H_2O_2 were inversely proportional to the FR levels of the sorted cell population (Figure 5C). Moreover, the FR of FR^{High} cells recovered to higher than basal levels after H_2O_2 exposure, indicating that FR^{High} cells have greater GSH-restoring capacity compared with control cells.

As shown in Figure 5D, the sorted hES-MSCs showed no significant difference in proliferation rate. When multipotency was examined, both FR^{High} and FR^{Low} cells exhibited a similar capacity to differentiate into chondrogenic, adipogenic, and osteogenic lineages (Figure S6A), but FR^{High} hES-MSCs, compared with FR^{Low} cells, showed a significant increase in the induction of some lineage markers, including *SOX9*, *AP2*, and *OCN* (Figure S6B). Additionally, FR^{High} hES-MSCs had approximately 4.7- and 4.9-fold higher numbers of CFU-F than did FR^{Mid} and FR^{Low} cells, respectively (Figure 5E). When individual CFU colonies were harvested and reseeded for limiting dilution assay, CFU colonies from FR^{High} hES-MSCs showed two times the clonogenic activity than those from FR^{Low} cells (Figure 5F), indicating the enhanced self-renewal activity of FR^{High} hES-MSCs. FR^{High} cells in both types of SCs showed significantly enhanced chemoattraction to stromal derived factor 1 compared with naive or FR^{Low} cells (Figure 5G). The improved chemotactic activities in FR^{High} cells were also found by PDGF stimuli and were significantly blocked by a PDGF receptor (PDGFR) inhibitor, STI571 (Figure 5H). Accordingly, FR^{High} hES-MSCs showed significantly higher mRNA levels of pluripotency- or migration-related genes than did naive and FR^{Low} cells, including *OCT4* and *CXCR4* (Figure 5I).

To prove the functional role of high GSH levels, we depleted cellular GSH in FR^{High} hES-MSCs using BSO and found that GSH depletion severely impaired the enhanced clonogenic and migration capacities as well as upregulation of the related genes observed in FR^{High} hES-MSCs (Figures 5J–5L, S6C, and S6D). In line with these data, declined cellular functions in FR^{Low} hES-MSCs were reversed to levels similar to those of FR^{High} cells by glutathione ethyl ester (GSH-EE), a cell-permeable glutathione. Moreover, naive cells treated with BSO and GSH-EE resulted in the significant repression and activation of chemoattraction to PDGF, respectively (Figure S6E).

To further investigate the significance of a high GSH content among other types of SC, we fractionated murine ESCs (mESCs) into higher- and lower-GSH level cells based on the FR of FreSHtracer (Figures 6A and 6B). Compared with FR^{Low} mESCs, FR^{High} cells displayed remarkably enhanced cellular function regarding GSH recovery capacity following H_2O_2 treatment (Figures 6C and 6D) and exhibited dome-like morphological colonies with positive alkaline phosphatase staining, characteristic of undifferentiated ESCs (Figure 6E). Additionally, FR^{High} mESCs were superior to FR^{Low} cells in terms of clonogenic efficiency as exhibited in the limiting dilution assay representing self-renewal activity (Figure 6F) and greater expression of pluripotency-related genes (Figures 6G and 6H). When they were differentiated by forming embryoid bodies (EBs), FR^{Low} mESCs exhibited defects in EB formation (Figure 6I) and induction of several lineage markers, such as neural (e.g., *Neurog2* and *Olig2*) and mesodermal (e.g., *T* and *Nkx2.5*) markers (Figures 6J and S6F). The defective differentiation capacity in cells from FR^{Low} EB was further validated by *in vitro* neuronal differentiation, evidenced by a lack of $\beta III\text{-tubulin}^+$ neurons (Figure 6K) and by impaired induction of neuronal markers (Figure 6L). Taken together, these findings demonstrate that high cellular GSH levels are required for maintaining the core functions in SCs.

GSH^{High} Stem Cells Show Higher Therapeutic Effectiveness in a Mouse Model of Asthma

To confirm these results *in vivo*, we compared the therapeutic effectiveness of FR^{High} and FR^{Low} hES-MSCs in a mouse model of virus-associated asthma. The mice were sensitized and challenged with ovalbumin and poly(I:C) and then injected with the sorted or naive hES-MSCs via the tail vein (Figure 7A). Histological examination showed that inflammatory responses were markedly attenuated around the bronchial and perivascular areas in the lungs of the FR^{High} cell-injected mice compared with those of the FR^{Low} or naive cell-injected mice (Figure 7B). The number of inflammatory cells in the bronchoalveolar lavage fluid from

(E and F) Effect of cell confluence and passage on the FR. HeLa cells (1×10^4, 2×10^4, and 4×10^4 cells/cm^2) were cultured for 24 hr and incubated with FreSHtracer (5 μM, 2 hr), followed by confocal microscopy analysis (E, upper). The FR within whole cells, the cytoplasm, and the nucleoplasm was analyzed (n = 30 cells from n = 3 independent experiments; E, lower). hBM-MSCs were subcultured from passage number (P) 4.5 to 6 by seeding at three different densities (1×10^3, 2×10^3, and 4×10^3 cells/cm^2) and cultured for 3 days, following equilibration with FreSHtracer (2 μM, 2 hr; F, left). The cells were analyzed using flow cytometry (F, right).
For all bar graphs, values represent mean ± SEM; *p < 0.05, **p < 0.01, ***p < 0.001. Scale bars, 10 μm (A, C, D, E).

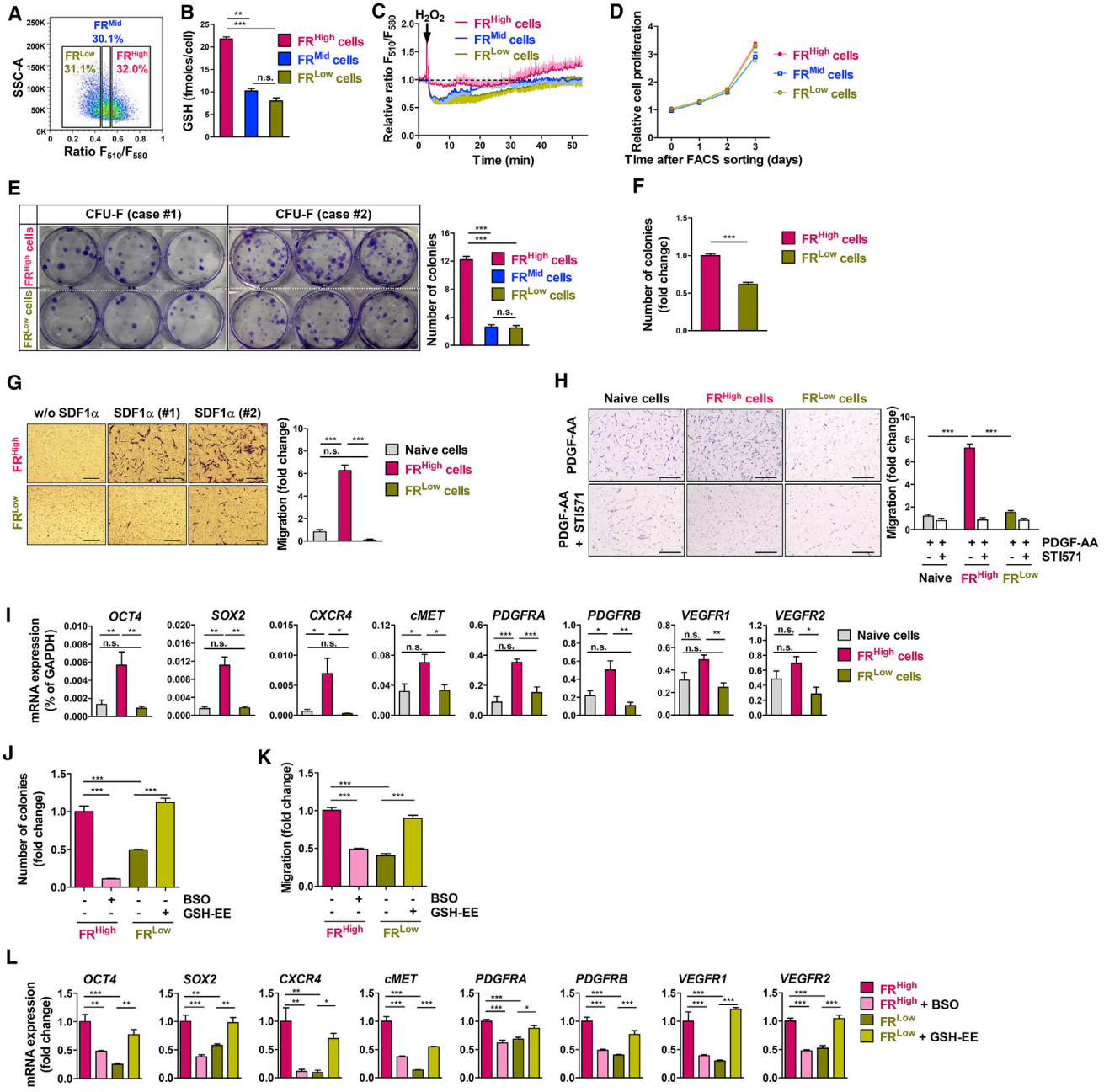

Figure 5. Intracellular GSH Levels Modulate the Self-Renewal and Migration Activities of Mesenchymal Stem Cells

(A) Sorting of hES-MSCs according to the F_{510}/F_{580} ratio (FR) into three populations: FR^{High}, FR^{Mid}, and FR^{Low} cells. Cells were characterized as described below, following the removal of FreSHtracer.

(B and C) Luminescence-based quantification of GSH in cell lysates (n = 2 independent biological replicates; B) and comparison of FR changes following treatment with 100 μM H_2O_2 (n = 3 cells; C) in FR^{High}, FR^{Mid}, and FR^{Low} hES-MSCs.

(D–I) Analyses of cell proliferation (n = 6 independent biological replicates; D), colony-forming unit fibroblasts (CFU-F; n = 15 independent biological replicates; E), limiting dilution by replating primary CFU colonies (n = 6 independent biological replicates; F), chemotaxis to stromal derived factor-1α (SDF1α; 150 ng/mL, n = 8 independent biological replicates; G), chemotaxis to 10 ng/mL platelet-derived growth factor (PDGF)-AA in the absence or presence of STI571 (0.5 μg/mL), a PDGFR inhibitor (n = 8 independent biological replicates; H), and qPCR of *OCT4*, *SOX2*, *CXCR4*, *cMET*, *PDGFRA*, *PDGFRB*, *VEGFR1*, and *VEGFR2* (n = 8 independent biological replicates; I) in hES-MSCs sorted based on the FR and in unsorted control (naive) cells.

(legend continued on next page)

FR^{High} cell-injected mice was lower than that from FR^{Low} or naive cell-injected mice (Figure 7C). Similarly, tumor necrosis factor α (TNF-α) and interleukin-17 (IL-17) levels were lower, whereas IL-10 levels were higher in the bronchoalveolar lavage fluid from FR^{High} cell-injected mice (Figure 7D). qRT-PCR confirmed the significantly decreased mRNA levels of inflammatory cytokines in the lung tissues of FR^{High} cell-injected mice (Figure 7E). Moreover, immunohistochemical staining with human β_2-microglobulin antibody showed a marked increase of engrafted cells in the lungs of FR^{High} hES-MSC-injected mice, which were identified as type-2 alveolar cells by staining with anti-prosurfactant protein C (SFTPC) antibody (Figures 7F and S7). These results indicated that the injected hES-MSCs differentiated into the alveolar epithelium (Krause et al., 2001; Rojas et al., 2005), contributing to tissue regeneration. Taken together, these results suggest that GSH levels can be used as a marker to evaluate SC function for enhancing the therapeutic potency.

DISCUSSION

GSH, the most abundant non-protein thiol in cells, functions as a redox buffer, preventing oxidative damage and regulating redox signaling. Therefore, the intracellular GSH level has been used as an important indicator to assess the intensity of oxidative stress (Winterbourn and Hampton, 2008). Since GSH levels are continuously fluctuating, owing to its regeneration and increased *de novo* synthesis under oxidative stress conditions (Lu, 2013), the real-time monitoring of GSH levels is required for a detailed analysis of the strength and duration of oxidative damage and consequent redox signaling. In the present study, we demonstrated that FreSHtracer, a chemical probe with the ability to undergo reversible addition reactions with thiols, can be used to monitor and measure GSH levels in living cells. The reaction with GSH induces changes in the fluorescence excitation and emission of the probe, which enables the ratiometric measurement of GSH, thus excluding the possible errors caused by different uptake of the FreSHtracer dye for individual cells and a specific organelle. FreSHtracer readily penetrates through cell membranes, and can report GSH levels with no cytotoxicity under both physiological and various ROS-generating conditions. More importantly, our detail *in vitro* kinetic and *in vivo* cellular studies showed that the FreSHtracer probe can successfully distinguish GSH from protein thiols (Figures 1 and 3). This simple, rapid, and ratiometric method is well suited for studying GSH dynamics of SCs using various techniques, including microscopic and flow-cytometric analyses.

Our results showed that GSH levels are much higher in the nucleus than in the cytosol, as proposed previously (García-Giménez et al., 2013). In addition, GSH levels decreased in the nucleus and cytosol to a similar extent, and maintained a concentration gradient under oxidative stress conditions, suggesting an unidentified mechanism that transports GSH into the nucleus against such a gradient. The maintenance of high GSH levels in the nucleus also suggests that GSH regulates DNA synthesis, transcription, and repair through modulation of redox signaling (García-Giménez et al., 2013).

Mitochondrial GSH (mGSH) constitutes 10%–15% of the total cellular GSH pool and is imported from the cytosol to play a major role in maintaining mitochondrial redox homeostasis (Mari et al., 2013). Our results with MitoFreSHtracer demonstrated that the mGSH levels differ among the mitochondria in a single cell. Such heterogeneity of mGSH levels might reflect differences in the activity of GSH transporters, rate of ROS production, and/or activity of NADPH production. With defects in these activities, depletion of mGSH results in DNA damage or apoptotic cell death and contributes to the pathogenesis of a number of diseases (Mari et al., 2013). Thus, MitoFreSHtracer could become an indispensable tool for investigating the regulation of mGSH in a variety of contexts.

A low ROS level is critical to preserve the self-renewal process of SCs (Mohyeldin et al., 2010) as well as to prevent mutations or damage that could impair their genetic and epigenetic integrity (Bigarella et al., 2014; Heo et al., 2017). Hematopoietic SCs with low ROS levels sorted by dichlorofluorescence staining exhibited long-term repopulating capacity (Jang and Sharkis, 2007). Consistently, we demonstrated that GSH levels were well correlated with the self-renewal activity of SCs. These results provide insight into the role of GSH in regulating redox signaling, which plays an important role in determining the SC fate, possibly modulating the activities of transcriptional factors such as NRF2 or FoxOs (Bigarella et al., 2014). Thus, monitoring of cellular GSH is necessary to evaluate SC function.

There is conflicting evidence on the role of ROS in the regulation of SC activities. ROS generated by Nox1 in

(J–L) Functional role of high GSH levels in hES-MSCs. CFU-F (n = 10 independent biological replicates; J), chemotaxis to 10 ng/mL PDGF-AA (n = 8 independent biological replicates; K), and qPCR assays of stemness and migration-related genes (n = 4 independent biological replicates; L) in control and BSO-treated FR^{High} hES-MSCs or control and GSH-EE supplemented FR^{Low} cells.
For all bar graphs, values represent mean ± SEM; *p < 0.05, **p < 0.01, ***p < 0.001; n.s., not significant. Scale bars, 200 μm (G and H).
See also Figures S5 and S6.

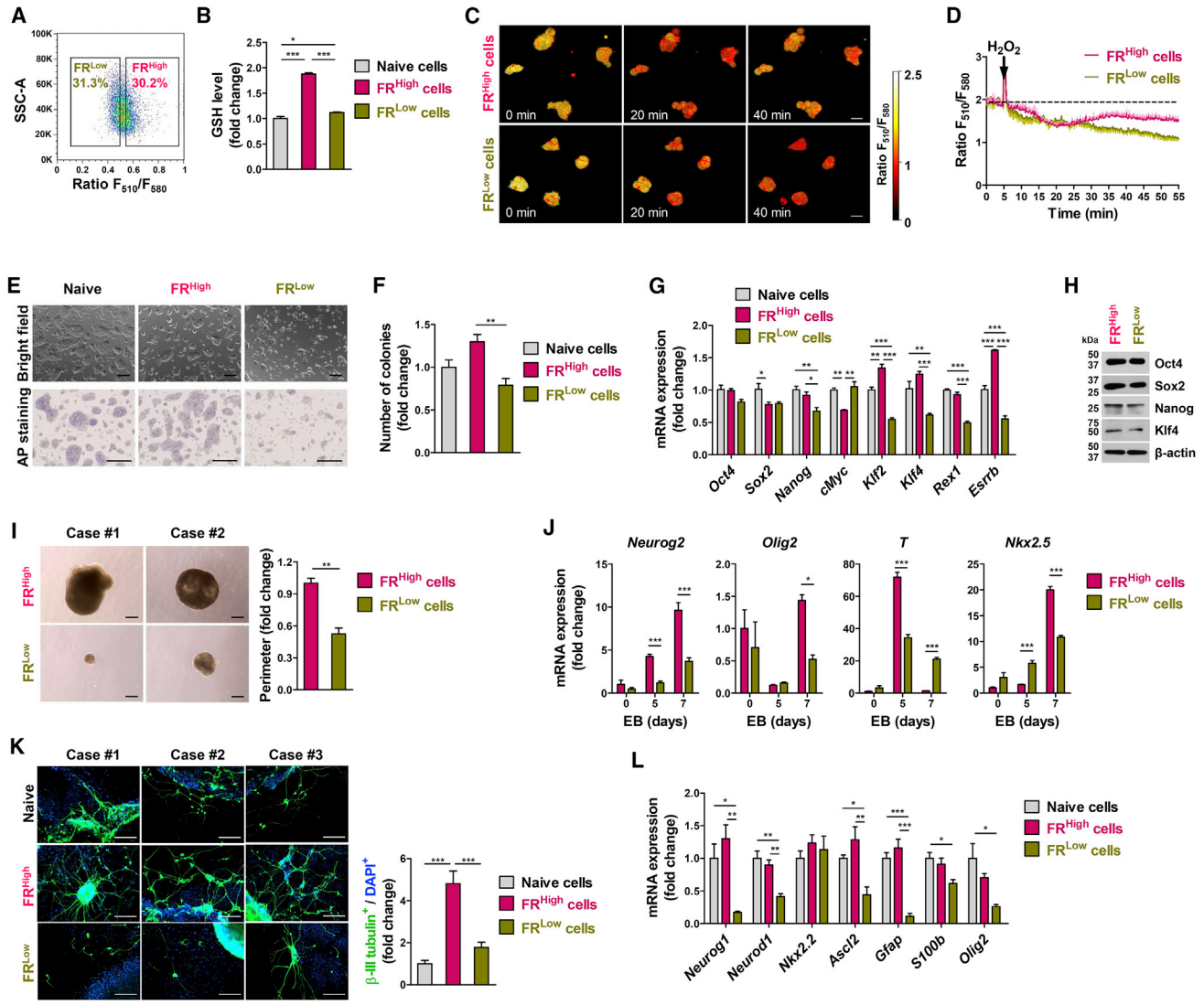

Figure 6. Impaired Pluripotency and Differentiation in Murine Embryonic Stem Cells with Low GSH Levels

(A) Sorting of murine ESCs (mESCs) according to the F_{510}/F_{580} ratio (FR) into FR^{High} and FR^{Low} populations.

(B) Luminescence-based quantification of GSH in cell lysates (n = 4 independent biological replicates).

(C and D) Representative pseudo-colored confocal images of the FR (C) and the comparison of their FR changes (n = 4 cells; D) in FR^{High} and FR^{Low} mESCs, following treatment with 100 μM H_2O_2. Scale bars, 10 μm.

(E) Representative pictures for bright-field (upper panel) and alkaline phosphatase (AP) staining (lower panel). Scale bars, 200 μm.

(F–H) Clonogenic capacity in limiting dilution (n = 5 independent biological replicates; F), qPCR (n = 4 independent biological replicates; G), and western blot (H) analyses in FR^{High} and FR^{Low} mESCs and in unsorted control (naive) cells.

(I) Representative pictures (left) and quantitation (n = 6 independent biological replicates; right) for size of 5-day embryoid body (EB) formed from FR^{High} and FR^{Low} mESCs. Scale bars, 200 μm.

(J) qPCR analyses for lineage-specific genes (*Neurog2*, *Olig2*, *T*, and *Nkx2.5*) in EBs at the indicated day (n = 4 independent biological replicates).

(K and L) Immunostaining of βIII-tubulin$^+$ neuron cells (green; K) qPCR analyses of neural lineage markers (*Neurog1*, *Neurod1*, *Nkx2.2*, *Ascl2*, *Gfap*, *S100b*, and *Olig2*; n = 4 independent biological replicates; L) during ESC differentiation. Nuclei were counterstained with DAPI (blue; K). The βIII-tubulin$^+$ neuron cells were quantitated by their frequency in total DAPI$^+$ cells (n = 5 independent biological replicates; K, right panel). Scale bars, 100 μm.

Values represent mean ± SEM; *p < 0.05, **p < 0.01, ***p < 0.001. See also Figure S6.

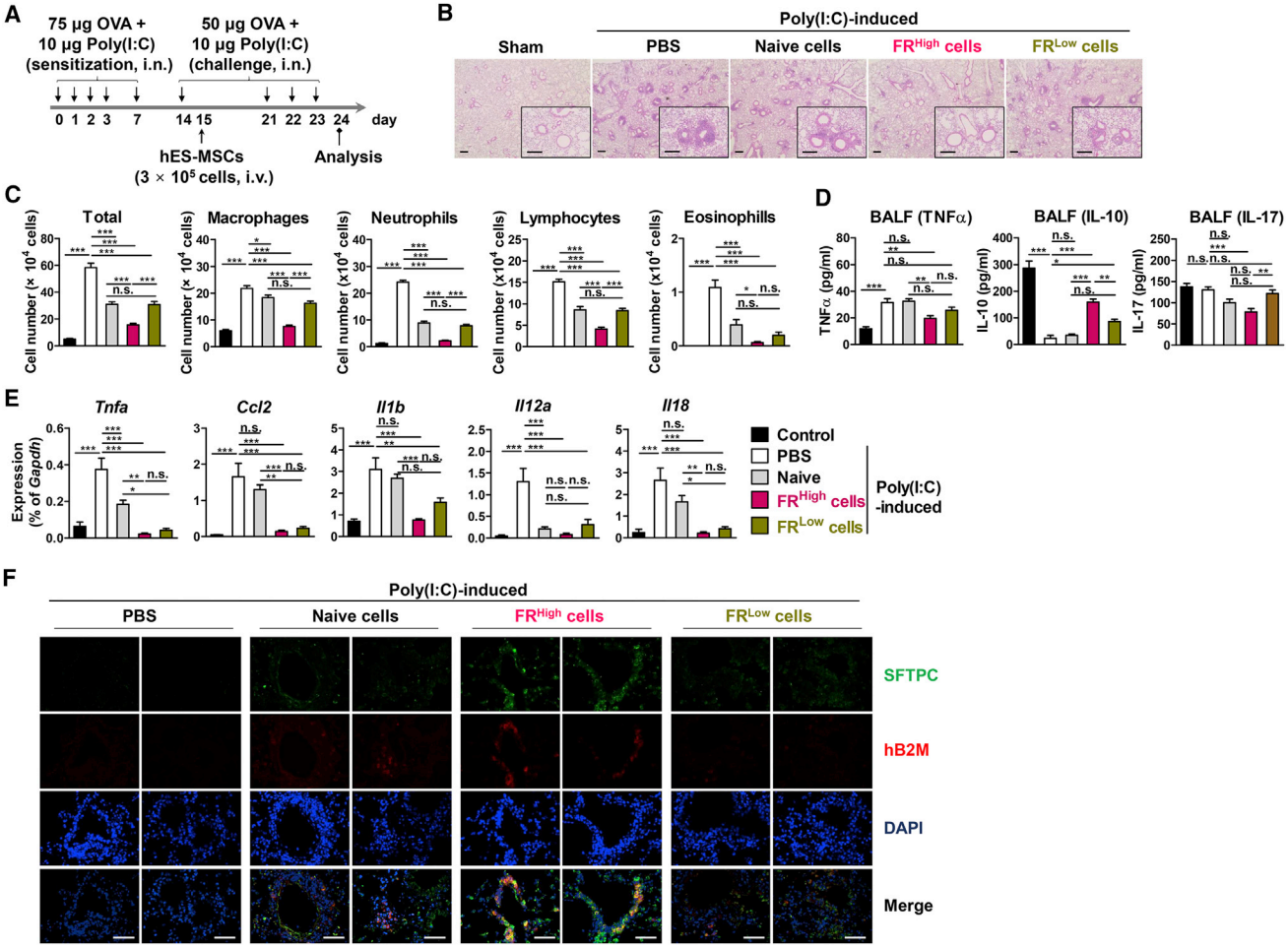

Figure 7. Stem Cells with High GSH Levels Exhibit Increased Therapeutic Efficacy

(A) Scheme for establishment of the poly(I:C)-induced mouse model of asthma.

(B–F) Naive, FR^{High}, and FR^{Low} hES-MSCs, or PBS were administered to mice treated with ovalbumin (OVA) and poly(I:C). (B) H&E staining of lung tissues. Sham, sham-operated. (C) Number of total cells, macrophages, neutrophils, lymphocytes, and eosinophils (n = 30 independent biological replicates from n = 10 mice) and (D) ELISA-based detection of TNF-α, IL-10, and IL-17 in the bronchoalveolar lavage fluid (n = 10 independent biological replicates from n = 10 mice). (E) qPCR analysis of *Tnfa*, *Ccl2*, *Il1b*, *Il12a*, and *Il18* expression using RNA isolated from the lung tissues (n = 10 independent biological replicates from n = 10 mice). (F) Immunofluorescent staining of human β-2 microglobulin expression (hB2M, red) and prosurfactant protein C (SFTPC, green) in the lung tissues. Nuclei were stained with DAPI (blue). For all bar graphs, values represent mean ± SEM; *p < 0.05, **p < 0.01, ***p < 0.001; n.s., not significant. Scale bars, 200 μm (B and F). See also Figure S7.

neural SCs or by Nox2 in spermatogonial SCs were shown to be required for their self-renewal activity (Le Belle et al., 2011; Morimoto et al., 2013). In contrast, ROS exhibited inhibitory effects on SC function (Kim and Wong, 2009; Nakamura et al., 2010). In addition, the defective hematopoietic SC functions observed in *Nrf2*-deficient mice were found to be independent of the ROS level (Merchant et al., 2011). These seemingly contradictory results might be attributed to microenvironment- and cell-type-specific mechanisms. Embryonic or quiescent adult SCs minimize ROS production by residing within a specialized niche with a relatively low oxygen concentration (1%–8%) in the body (Mohyeldin et al., 2010) and by depending on anaerobic glycolysis through low mitochondrial biogenesis (Ito and Suda, 2014). Moreover, in the present study, GSH^{High} SCs exhibited greater GSH-regenerating activity than GSH^{Low} SCs (Figures 5C and 6D). Therefore, the intrinsic activities of GSH synthesis and regeneration, rather than the amount of ROS produced, are responsible for determining the effect of ROS on cellular function.

Flow-cytometric analysis of SC populations revealed substantial heterogeneity of GSH levels among individual cells,

and GSH^{High} cell fractionation using FreSHtracer showed the enhanced functionalities evidenced in both *in vitro* and *in vivo* analyses. Importantly, we found that this heterogeneity of GSH levels changed in the SC population with increasing passage numbers (Figure 4F). These findings indicate that SCs respond differently to oxidative stress even under exposure to an atmospheric oxygen concentration (21%). Further work is needed to investigate the mechanism by which GSH levels are differentially regulated in SCs in response to ROS. FreSHtracer is a useful tool for the real-time monitoring of intracellular GSH levels in living SCs and for fractionating cells according to their GSH levels. Comparison of the signaling pathways between GSH^{High} and GSH^{Low} cells could be helpful in identifying the key players involved in the GSH regulation of SCs.

In summary, we demonstrated that FreSHtracer could be used for studying various aspects of GSH homeostasis, including synthesis, transport, and regeneration. Spatiotemporal information regarding intracellular GSH levels in living cells might facilitate detailed investigations into the molecular mechanisms contributing to altered cellular functions in response to internal and external stresses. During the preparation of this paper, recent studies also reported very similar coumarin derivatives for the monitoring of GSH levels inside HeLa cells (Chen et al., 2017; Jiang et al., 2017).

EXPERIMENTAL PROCEDURES

Detailed methods are provided in Supplemental Experimental Procedures.

Cell Lines and Culture

HeLa and RAW264.7 cells were purchased from the Korean Cell Line Bank (Seoul, Korea) and the American Type Culture Collection (ATCC; Manassas, VA), respectively. The cells were grown in phenol red-free DMEM (Welgene, LM 001-10; Gyeongsan, Korea) supplemented with 10% heat-inactivated fetal bovine serum (HyClone; GE Healthcare, Melbourne, VIC, Australia), 100 U/mL penicillin, 100 μg/mL streptomycin sulfate, and 2 mM glutamine. hES-MSCs were kindly provided by Hyung-Min Chung (Konkuk University, Korea). Cellular GSH of hES-MSCs was depleted by treating cells with 80 μM BSO (Sigma-Aldrich, St. Louis, MO) for 24 hr and was restored with 1 mM GSH-EE (Sigma-Aldrich) for 2 hr, followed by their functional assays. hBM-MSCs (Lonza, Walkersville, MD) were cultured according to the manufacturer's instructions. Culture, EB formation, and *in vitro* neuronal differentiation of murine E14TG2a ESCs (ATCC) were performed as previously described (Heo et al., 2017).

Confocal Imaging of the Fluorescence Ratio within Living Cells

HeLa cells (1.8×10^5 cells/dish), RAW264.7 cells (2×10^5 cells/dish), hBM-MSCs (8×10^4 cells/dish), hES-MSCs (1.5×10^5 cells/dish), and murine E14TG2a ESCs (5×10^5 cells/dish) were seeded onto 35-mm coverglass-bottom dishes (SPL Life Sciences, Pocheon, Korea) and cultured at 37°C in a 5% CO_2 incubator for 16–20 hr. The cells were then equilibrated with 5 μM FreSHtracer in 2 mL of culture medium, followed by microscopic analysis. For mitochondrial GSH imaging, HeLa cells were incubated with 10 μM MitoFreSHtracer for 1.5 hr, washed twice with PBS, and analyzed in 2 mL of fresh culture medium using a confocal microscope. Time-lapse imaging of the cells was performed using a Nikon A1 laser-scanning confocal microscope. The cells were maintained at 37°C in a 5% CO_2 atmosphere by a stage-top incubator. The chamber was mounted on a Nikon ECLIPSE Ti inverted microscope, equipped with a CFI Plan apochromat 60×, 1.40-numerical aperture (NA) objective (oil immersion) or a CFI Plan apochromat 20×, 0.8-NA objective. FreSHtracer was excited by lasers at 405 nm and 488 nm, and the emissions were detected through 500- to 550-nm and 570- to 620-nm band-pass filters. Cells in the focused area were gently treated with 20 μL of 100× concentrated solutions of H_2O_2, diamide, or DTT. Data were analyzed and pseudo-color ratio images were generated using NIS-Elements AR software. FreSHtracer was prepared according to our previously reported method (Cho and Choi, 2012). This probe is now commercially available (Cell2in, Seoul, Korea).

Animal Study Approval

All animal experiments were approved and performed in accordance with guidelines set by the Institutional Animal Care and Use Committee of the University of the Ulsan College of Medicine (2015-12-061).

Statistical Analysis

We used a two-sided t test for single pairwise comparisons. We also used one-way ANOVA with a Tukey post hoc test for multiple comparisons. Values are expressed as the mean and SEM. All statistical analyses were performed using GraphPad Prism 5 software.

SUPPLEMENTAL INFORMATION

Supplemental Information includes Supplemental Experimental Procedures, seven figures, and one table and can be found with this article online at https://doi.org/10.1016/j.stemcr.2017.12.007.

AUTHOR CONTRIBUTIONS

E.M.J., K.C., and D-.M.S. designed the experiments; E.M.J., J-.H.Y., J.L., J-.W.S., A.Y.C., J.H., K.B.L., J-.H.L., W.J.L., H-.J.K., Y.H.S., S-.J.L., S-.Y.C., and K.C. performed the experiments; E.M.J., D-.M.S., K.C., and I-.G.K. wrote the paper.

ACKNOWLEDGMENTS

We thank Dr. Hyung-Min Chung for providing the hES-MSCs, Hyewon Kang for assisting with the stem cell experiments, and the staff of the Biomedical Imaging Center and FACS Center of the Core Research Facilities of Seoul National University College of Medicine for their technical advice and assistance. This work was funded by the National Research Foundation of Korea through the Basic Science Research Program (NRF-2013R1A1A2065273,

NRF-2014R1A2A2A01006731, NRF-2014R1A1A2055832, NRF-2017R1D1A1B03035059, and NRF-2017M3A9B4061890); the Korea Healthcare Technology R&D Project, Ministry of Health and Welfare, Republic of Korea (HI10C0185 and HI14C3339); and the Brain Korea 21 PLUS program of the Korean Ministry of Education, Science and Technology. I-.G.K., K.C., D-.M.S., E.M.J., and J-.W.S. co-founded Cell2in, a company developing cell therapy using FreSHtracer.

Received: August 4, 2017
Revised: December 5, 2017
Accepted: December 6, 2017
Published: January 4, 2018

REFERENCES

Balaban, R.S., Nemoto, S., and Finkel, T. (2005). Mitochondria, oxidants, and aging. Cell *120*, 483–495.

Bigarella, C.L., Liang, R., and Ghaffari, S. (2014). Stem cells and the impact of ROS signaling. Development *141*, 4206–4218.

Chen, J., Jiang, X., Carroll, S., Huang, J., and Wang, J. (2015). Theoretical and experimental investigation of thermodynamics and kinetics of thiol-Michael addition reactions: a case study of reversible fluorescent probes for glutathione imaging in single cells. Org. Lett. *17*, 5978–5981.

Chen, J., Jiang, X., Zhang, C., MacKenzie, K.R., Stossi, F., Palzkill, T., Wang, M.C., and Wang, J. (2017). Reversible reaction-based fluorescent probe for real-time imaging of glutathione dynamics in mitochondria. ACS Sens. *2*, 1257–1261.

Cho, A.Y., and Choi, K. (2012). A coumarin-based fluorescence sensor for the reversible detection of thiols. Chem. Lett. *41*, 1611–1612.

Dannenmann, B., Lehle, S., Hildebrand, D.G., Kubler, A., Grondona, P., Schmid, V., Holzer, K., Froschl, M., Essmann, F., Rothfuss, O., et al. (2015). High glutathione and glutathione peroxidase-2 levels mediate cell-type-specific DNA damage protection in human induced pluripotent stem cells. Stem Cell Reports *4*, 886–898.

Drose, S., and Brandt, U. (2008). The mechanism of mitochondrial superoxide production by the cytochrome bc1 complex. J. Biol. Chem. *283*, 21649–21654.

Finka, A., and Goloubinoff, P. (2013). Proteomic data from human cell cultures refine mechanisms of chaperone-mediated protein homeostasis. Cell Stress Chaperones *18*, 591–605.

García-Giménez, J.L., Markovic, J., Dasí, F., Queval, G., Schnaubelt, D., Foyer, C.H., and Pallardó, F.V. (2013). Nuclear glutathione. Biochim. Biophys. Acta *1830*, 3304–3316.

Gutscher, M., Pauleau, A.L., Marty, L., Brach, T., Wabnitz, G.H., Samstag, Y., Meyer, A.J., and Dick, T.P. (2008). Real-time imaging of the intracellular glutathione redox potential. Nat. Methods *5*, 553–559.

Hansen, R.E., Roth, D., and Winther, J.R. (2009). Quantifying the global cellular thiol-disulfide status. Proc. Natl. Acad. Sci. USA *106*, 422–427.

Heo, J., Lim, J., Lee, S., Jeong, J., Kang, H., Kim, Y., Kang, J.W., Yu, H.Y., Jeong, E.M., Kim, K., et al. (2017). Sirt1 regulates DNA methylation and differentiation potential of embryonic stem cells by antagonizing Dnmt3l. Cell Rep. *18*, 1930–1945.

Hochmuth, C.E., Biteau, B., Bohmann, D., and Jasper, H. (2011). Redox regulation by Keap1 and Nrf2 controls intestinal stem cell proliferation in Drosophila. Cell Stem Cell *8*, 188–199.

Hong, K.S., Bae, D., Choi, Y., Kang, S.W., Moon, S.H., Lee, H.T., and Chung, H.M. (2015). A porous membrane-mediated isolation of mesenchymal stem cells from human embryonic stem cells. Tissue Eng. Part C Methods *21*, 322–329.

Ito, K., and Suda, T. (2014). Metabolic requirements for the maintenance of self-renewing stem cells. Nat. Rev. Mol. Cell Biol. *15*, 243–256.

Jang, J., Wang, Y., Kim, H.S., Lalli, M.A., and Kosik, K.S. (2014). Nrf2, a regulator of the proteasome, controls self-renewal and pluripotency in human embryonic stem cells. Stem Cells *32*, 2616–2625.

Jang, Y.Y., and Sharkis, S.J. (2007). A low level of reactive oxygen species selects for primitive hematopoietic stem cells that may reside in the low-oxygenic niche. Blood *110*, 3056–3063.

Jiang, X., Chen, J., Bajić, A., Zhang, C., Song, X., Carroll, S.L., Cai, Z.L., Tang, M., Xue, M., Cheng, N., et al. (2017). Quantitative real-time imaging of glutathione. Nat. Commun. *8*, 16087.

Kim, G.J., Lee, K., Kwon, H., and Kim, H.J. (2011). Ratiometric fluorescence imaging of cellular glutathione. Org. Lett. *13*, 2799–2801.

Kim, J., and Wong, P.K. (2009). Loss of ATM impairs proliferation of neural stem cells through oxidative stress-mediated p38 MAPK signaling. Stem Cells *27*, 1987–1998.

Krause, D.S., Theise, N.D., Collector, M.I., Henegariu, O., Hwang, S., Gardner, R., Neutzel, S., and Sharkis, S.J. (2001). Multi-organ, multi-lineage engraftment by a single bone marrow-derived stem cell. Cell *105*, 369–377.

Le Belle, J.E., Orozco, N.M., Paucar, A.A., Saxe, J.P., Mottahedeh, J., Pyle, A.D., Wu, H., and Kornblum, H.I. (2011). Proliferative neural stem cells have high endogenous ROS levels that regulate self-renewal and neurogenesis in a PI3K/Akt-dependant manner. Cell Stem Cell *8*, 59–71.

Lu, S.C. (2013). Glutathione synthesis. Biochim. Biophys. Acta *1830*, 3143–3153.

Mari, M., Morales, A., Colell, A., Garcia-Ruiz, C., Kaplowitz, N., and Fernandez-Checa, J.C. (2013). Mitochondrial glutathione: features, regulation and role in disease. Biochim. Biophys. Acta *1830*, 3317–3328.

Marsboom, G., Zhang, G.F., Pohl-Avila, N., Zhang, Y., Yuan, Y., Kang, H., Hao, B., Brunengraber, H., Malik, A.B., and Rehman, J. (2016). Glutamine metabolism regulates the pluripotency transcription factor OCT4. Cell Rep. *16*, 323–332.

Merchant, A.A., Singh, A., Matsui, W., and Biswal, S. (2011). The redox-sensitive transcription factor Nrf2 regulates murine hematopoietic stem cell survival independently of ROS levels. Blood *118*, 6572–6579.

Mohyeldin, A., Garzon-Muvdi, T., and Quinones-Hinojosa, A. (2010). Oxygen in stem cell biology: a critical component of the stem cell niche. Cell Stem Cell *7*, 150–161.

Morimoto, H., Iwata, K., Ogonuki, N., Inoue, K., Atsuo, O., Kanatsu-Shinohara, M., Morimoto, T., Yabe-Nishimura, C., and

Shinohara, T. (2013). ROS are required for mouse spermatogonial stem cell self-renewal. Cell Stem Cell *12*, 774–786.

Murphy, M.P., and Smith, R.A. (2007). Targeting antioxidants to mitochondria by conjugation to lipophilic cations. Annu. Rev. Pharmacol. Toxicol. *47*, 629–656.

Nakamura, B.N., Lawson, G., Chan, J.Y., Banuelos, J., Cortes, M.M., Hoang, Y.D., Ortiz, L., Rau, B.A., and Luderer, U. (2010). Knockout of the transcription factor NRF2 disrupts spermatogenesis in an age-dependent manner. Free Radic. Biol. Med. *49*, 1368–1379.

Paul, M.K., Bisht, B., Darmawan, D.O., Chiou, R., Ha, V.L., Wallace, W.D., Chon, A.T., Hegab, A.E., Grogan, T., Elashoff, D.A., et al. (2014). Dynamic changes in intracellular ROS levels regulate airway basal stem cell homeostasis through Nrf2-dependent Notch signaling. Cell Stem Cell *15*, 199–214.

Rojas, M., Xu, J., Woods, C.R., Mora, A.L., Spears, W., Roman, J., and Brigham, K.L. (2005). Bone marrow-derived mesenchymal stem cells in repair of the injured lung. Am. J. Respir. Cell Mol. Biol. *33*, 145–152.

Tsai, J.J., Dudakov, J.A., Takahashi, K., Shieh, J.H., Velardi, E., Holland, A.M., Singer, N.V., West, M.L., Smith, O.M., Young, L.F., et al. (2013). Nrf2 regulates haematopoietic stem cell function. Nat. Cell Biol. *15*, 309–316.

Umezawa, K., Yoshida, M., Kamiya, M., Yamasoba, T., and Urano, Y. (2017). Rational design of reversible fluorescent probes for live-cell imaging and quantification of fast glutathione dynamics. Nat. Chem. *9*, 279–286.

Wang, K., Zhang, T., Dong, Q., Nice, E.C., Huang, C., and Wei, Y. (2013). Redox homeostasis: the linchpin in stem cell self-renewal and differentiation. Cell Death Dis. *4*, e537.

Winterbourn, C.C., and Hampton, M.B. (2008). Thiol chemistry and specificity in redox signaling. Free Radic. Biol. Med. *45*, 549–561.

Yin, C., Huo, F., Zhang, J., Martinez-Manez, R., Yang, Y., Lv, H., and Li, S. (2013). Thiol-addition reactions and their applications in thiol recognition. Chem. Soc. Rev. *42*, 6032–6059.

Stem Cell Reports, Volume *10*

Supplemental Information

Real-Time Monitoring of Glutathione in Living Cells Reveals that High Glutathione Levels Are Required to Maintain Stem Cell Function

Eui Man Jeong, Ji-Hye Yoon, Jisun Lim, Ji-Woong Shin, A. Young Cho, Jinbeom Heo, Ki Baek Lee, Jin-Haeng Lee, Won Jong Lee, Hyo-Jun Kim, Young Hoon Son, Seok-Jin Lee, Sung-Yup Cho, Dong-Myung Shin, Kihang Choi, and In-Gyu Kim

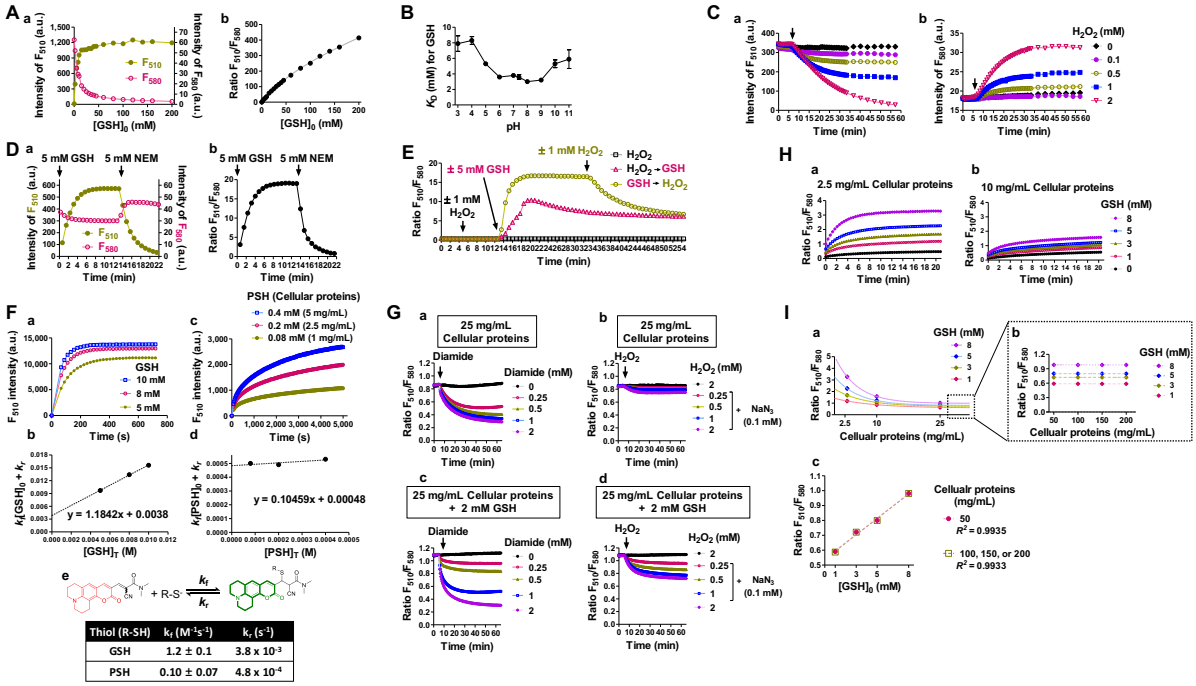

Thiol (R-SH)	k_f ($M^{-1}s^{-1}$)	k_r (s^{-1})
GSH	1.2 ± 0.1	3.8×10^{-3}
PSH	0.10 ± 0.07	4.8×10^{-4}

Figure S1. Properties of FreSHtracer as a Reversible and Ratiometric Glutathione (GSH) Sensor, Related to Figure 1

(A) Relationship between the fluorescence intensity of FreSHtracer and the GSH concentration. (a) Fluorescence emission intensities of FreSHtracer, at 510 nm (F_{510}) and 580 nm (F_{580}), plotted against the GSH concentration. (b) F_{510}/F_{580} ratio (FR) plotted against the GSH concentration. The corresponding fluorescence spectra are shown in Figure 1A.

(B) Effects of pH on the K_D of FreSHtracer for GSH. The K_D values were calculated using SigmaPlot 2000 (SPSS; See **Supplemental Experimental Procedures**).

(C) FreSHtracer (10 μM) was reacted with 5 mM GSH for 20 min. Following treatment with the indicated concentrations of H_2O_2 at room temperature, (a) F_{510} and (b) F_{580} were monitored. The corresponding FR values are shown in Figure 1D.

(D) Rapid and reversible changes of FreSHtracer fluorescence following treatment with GSH or *N*-ethylmaleimide (NEM). (a,b) FreSHtracer was reacted at room temperature (RT), first with 5 mM GSH, and then with 5 mM NEM. The reaction was monitored by recording the F_{510} and F_{580} values (a) and by calculating the FR (b).

(E) FreSHtracer was incubated sequentially with 1 mM H_2O_2 and 5 mM GSH, as indicated. The FR was monitored for 1 h.

(F) Rate constants for the reactions between FreSHtracer and thiols (See **Supplemental Experimental Procedures**). FreSHtracer was added to (a, b) GSH, or (c, d) dialyzed cell lysates (PSH), and F_{510} was monitored.

(e) The calculated rate constants

(G) Monitoring the FR of FreSHtracer in dialyzed cell lysates following treatment with diamide or H_2O_2. (a, b) In dialyzed cell lysates (25 mg/mL protein) equilibrated with FreSHtracer (10 μM, 2 h), the FR was monitored for 1 h following treatment with the indicated amounts of diamide or H_2O_2. (c, d) Dialyzed cell lysates (25 mg/mL protein) spiked with 2 mM GSH were equilibrated with FreSHtracer (10 μM; 2 h) and then the FR was monitored for 1 h following treatment with the indicated amounts of diamide or H_2O_2. Sodium azide was used to inhibit catalase activity in the dialyzed cell lysates (b, d). See also Figure 1H and 1K.

(H) Effect of PSH concentrations on FR_{GSH}. Dialyzed cell lysates (a, 2.5 mg/mL; b, 10 mg/mL) were spiked with various concentrations of GSH and were equilibrated with 10 μM FreSHtracer. The FR was monitored for 20 min. All reactions were performed at room temperature in 10 mM phosphate buffer (pH 7.4) containing 150 mM NaCl and 2% DMSO. a.u., arbitrary units. See also Figure 1I for 25 mg/mL cellular proteins and Figure 1J for the relationship between FR and GSH concentration in PSH-GSH mixtures.

(I) The F_{510}/F_{580} ratio becomes less sensitive at higher protein concentration ranges. All graphs are redrawn from Figure 1J. (a) The F_{510}/F_{580} ratios are curve-fitted and (b) extrapolated to the one phase decay model (GraphPad Prism 5.0): $Y = (Y_0 - \text{plateau}) * \exp(-K * X) + \text{plateau}$. (c) The calculated plateau ratios are plotted against the GSH concentrations. The ratio is expected to be linearly dependent on the GSH level, but not significantly affected by protein concentration changes (50—200 mg/mL).

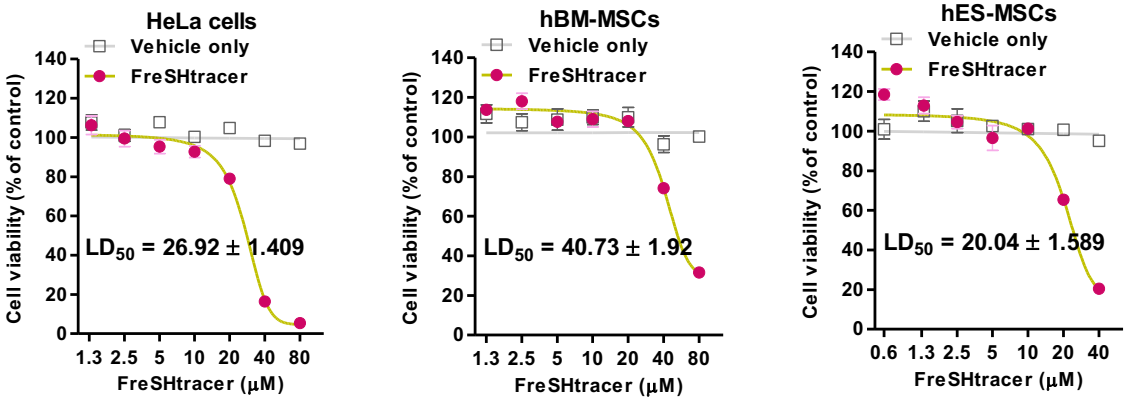

Figure S2. Effects of FreSHtracer on Cell Viability, Related to Figure 2

HeLa cells (5×10^3 cells/well; n = 3 independent biological replicates), hBM-MSCs (1.3×10^3 cells/well; n = 3 independent biological replicates), and hES-MSCs (1×10^4 cells/well; n = 3 independent biological replicates) were cultured for 18 h in 96-well dishes, and then treated for 24 h with either vehicle (dimethyl sulfoxide [DMSO]) or the indicated concentrations of FreSHtracer. Cell viability was analyzed using the MTT method. The LD_{50} values for FreSHtracer were calculated using GraphPad Prism 5. All error bars represent the mean ± SEM.

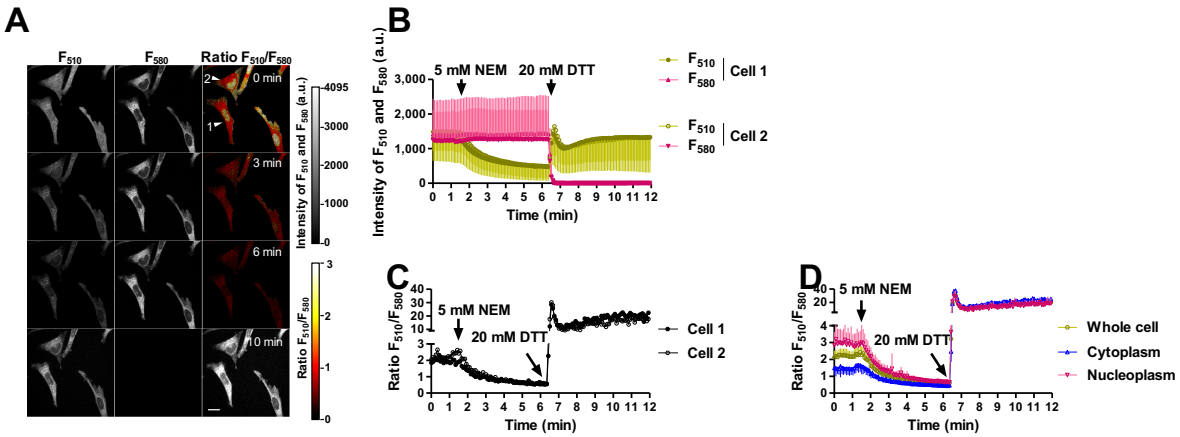

Figure S3. Reversible Reaction of FreSHtracer with Intracellular Thiols in Living Cells, Related to Figure 2

HeLa cells were equilibrated for 2 h with 5 μM FreSHtracer, and fluorescence emission intensities were monitored at F_{510} and F_{580} at 5-s intervals after treatment with *N*-ethylmaleimide (NEM), followed by 0.5 mM dithiothreitol (DTT). The F_{510}/F_{580} ratio (FR) was calculated using the NIS-Elements AR software program.

(A) Confocal and pseudo-color images of FreSHtracer-loaded cells.

(B and C) The fluorescence emission intensities of two cells (arrowheads) were monitored (B) and calculated as the FR (C).

(D) The average FR in whole cells, the cytoplasm, and the nucleoplasm from four different cells. All error bars represent the mean ± SEM.

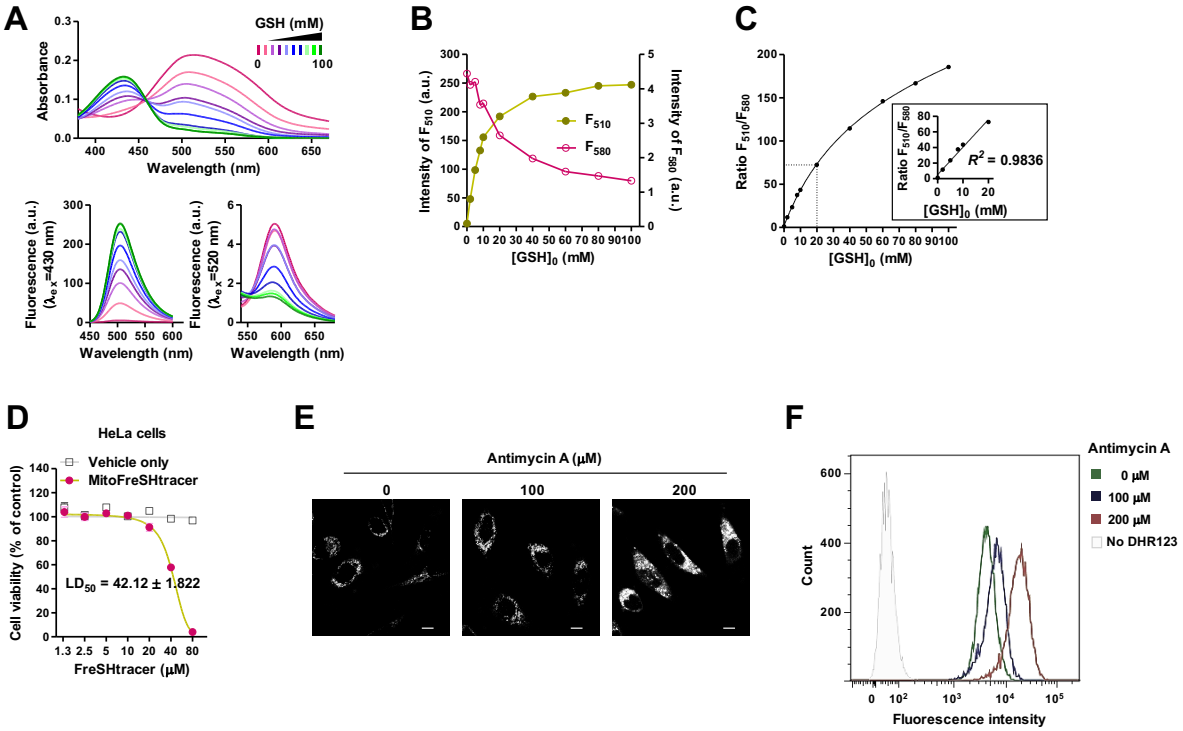

Figure S4. Characterization of MitoFreSHtracer, Related to Figure 2

(A–C) Spectroscopic properties of MitoFreSHtracer during the reaction with glutathione (GSH). Reactions were performed at room temperature in 10 mM phosphate buffer (pH 7.4) containing 150 mM NaCl and 2% dimethyl sulfoxide and monitored by ultraviolet-visible absorption spectroscopy. MitoFreSHtracer (10 μM) was reacted for 20 min with various concentrations of GSH ($[GSH]_0$ = 0–100 mM) (A). Fluorescence emission spectra of MitoFreSHtracer excited at 430 nm and 520 nm. Fluorescence intensities were plotted against the GSH concentration (B). The F_{510}/F_{580} ratio (FR) was calculated and plotted against the GSH concentration (C). A linear regression curve was fitted spanning the physiological range of GSH concentrations (0–20 mM; C, inset). a.u., arbitrary units.

(D) Effects of MitoFreSHtracer on cell viability. HeLa cells (5×10^3 cells/well; n = 3 independent biological replicates) were cultured for 18 h in 96-well dishes, and then treated for 24 h with either vehicle (dimethyl sulfoxide [DMSO]) or the indicated concentrations of FreSHtracer. Cell viability was analyzed using the MTT method. The LD_{50} values for FreSHtracer were calculated using GraphPad Prism 5. The error bars indicate the mean ± SEM.

(E and F) Measurement of the mitochondrial ROS generated by treatment with antimycin A. HeLa cells (1.8×10^4 cells/cm^2) were cultured for 18 h, and then incubated for 20 min with the indicated concentrations of antimycin A and 30 μM of dihydrorhodamine 123 (DHR123). Cells were washed twice with cold PBS, and analyzed in the presence of cold culture media by confocal microscopy (E) or with an LSR Fortessa flow cytometry system following trypsinization (F). Scale bar, 10 μm.

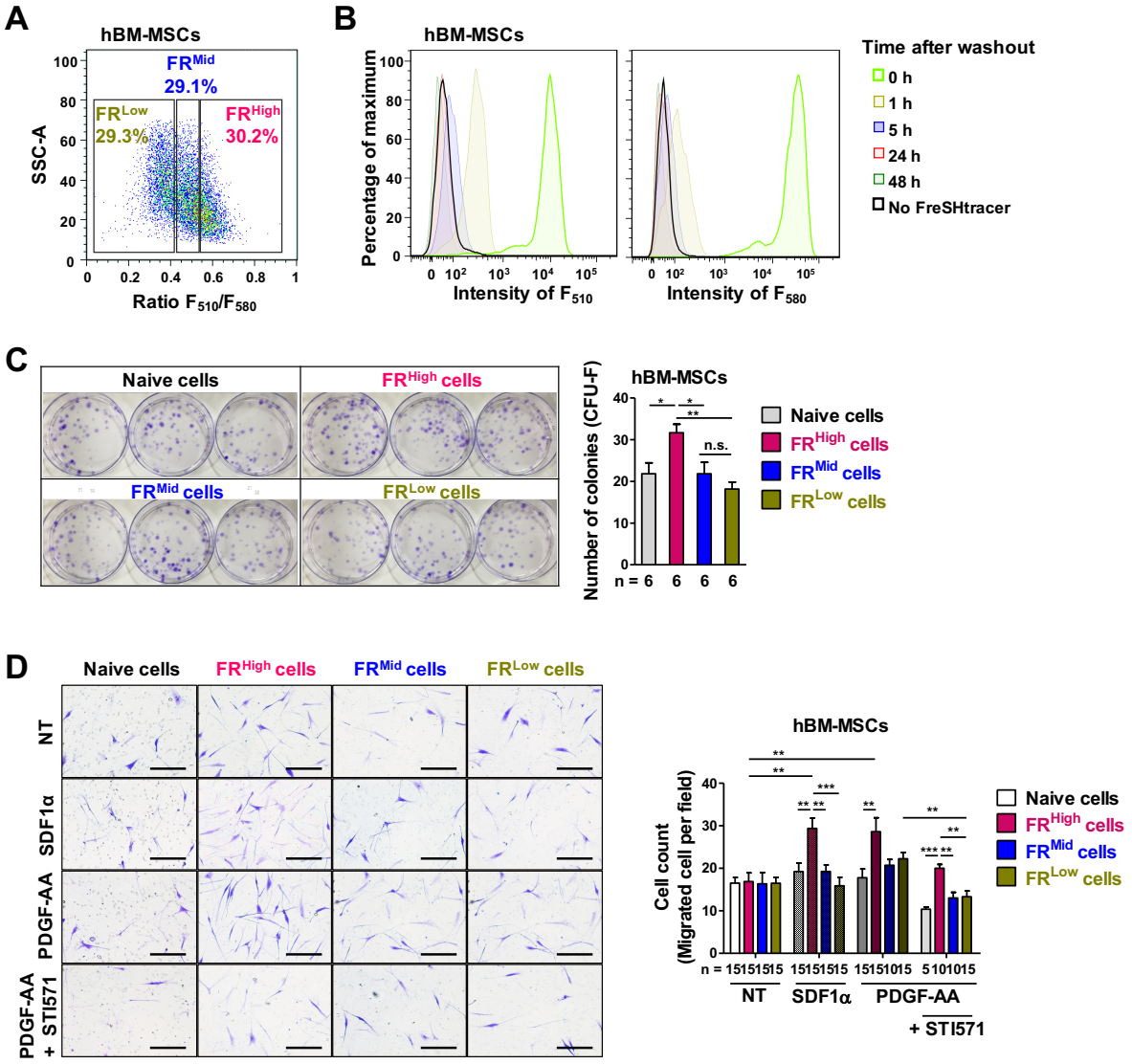

Figure S5. Characterization of Sorted hBM-MSCs According to F_{510}/F_{580} Ratio (FR) Values, Related to Figure 5

(A) Sorting of hBM-MSCs by FR into three populations: FR^{High}, FR^{Mid}, and FR^{Low} cells. Cells were characterized as described below, following the removal of FreSHtracer.

(B) Removal of FreSHtracer by PBS wash. hBM-MSCs were equilibrated with FreSHtracer (2 μM; 2 h), washed three times with PBS, and then cultured in growth media for the indicated times. Residual FreSHtracer in hBM-MSCs was measured by flow cytometry for F_{510} and F_{580}.

(C and D) Assays of colony-forming units-fibroblasts (CFU-F, n = 6 independent biological replicates; C) and chemotaxis (n = 5, 10, or 15 independent biological replicates; D) to stromal-derived factor 1-alpha (SDF1α, 150 ng/mL) and platelet-derived growth factor (PDGF)-AA (10 ng/mL) in the absence or presence of STI571 (0.5 μg/mL), a PDGFR inhibitor, for sorted hBM-MSCs according to FR and unsorted control (naive) cells. Scale bar, 200 μm. All error bars represent the mean ± SEM. $*P < 0.05$, $**P < 0.01$, $***P < 0.001$. n.s., not significant.

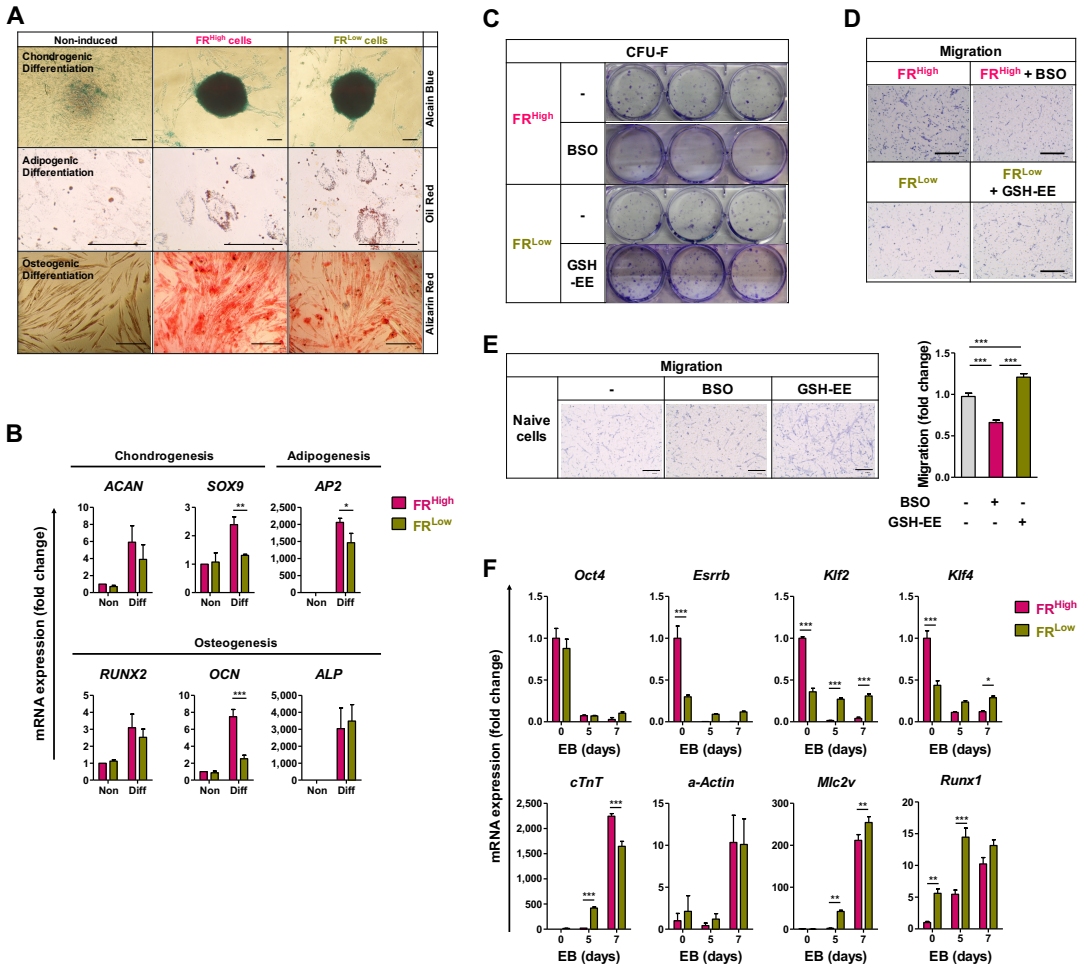

Figure S6. Cellular Functions of Sorted SCs According to F_{510}/F_{580} Ratio (FR) Values, Related to Figures 5 and 6

(A and B) Sorting of hES-MSC by FR into two populations: FR^{High} and FR^{Low} cells. Cells were cultured in chondrogenic, adipogenic, or osteogenic induction media. Cells were stained with Alcian Blue, Oil Red O, or Alizarin Red S (A). qPCR analysis (n = 4 independent biological replicates) to quantify lineage-specific genes in non-differentiated (Non) and differentiated (Diff) FR^{High} and FR^{Low} cells (B).

(C and D) Representative images for colony-forming unit fibroblasts assay (CFU-F, C) and chemotaxis assay to 10 ng/mL platelet-derived growth factor (PDGF)-AA (D) in FR^{High} and FR^{Low} hES-MSCs treated with BSO and GSH-EE, respectively. The corresponding graphs are shown in Figure 5J and 5K, respectively.

(E) Analyses of chemotaxis to 10 ng/mL PDGF-AA (n = 10 independent biological replicates) in unsorted control (naive) hES-MSCs treated with BSO or GSH-EE. Quantitative data are represented as the ratio to non-treated naive cells.

(F) mESC sorted by FR into two populations (FR^{High} and FR^{Low} cells) were differentiated by forming embryoid body (EB). qPCR analyses (n = 4 independent biological replicates) of the pluripotency and lineage-specific genes in cells from EB were performed at the indicated day. Quantitative data are represented as the ratio to FR^{High} cells of day 0. All error bars represent the mean ± SEM. $*P < 0.05$, $**P < 0.01$, $***P < 0.001$, one- or two-way ANOVA with Bonferroni post-hoc tests. Scale bar, 200 μm.

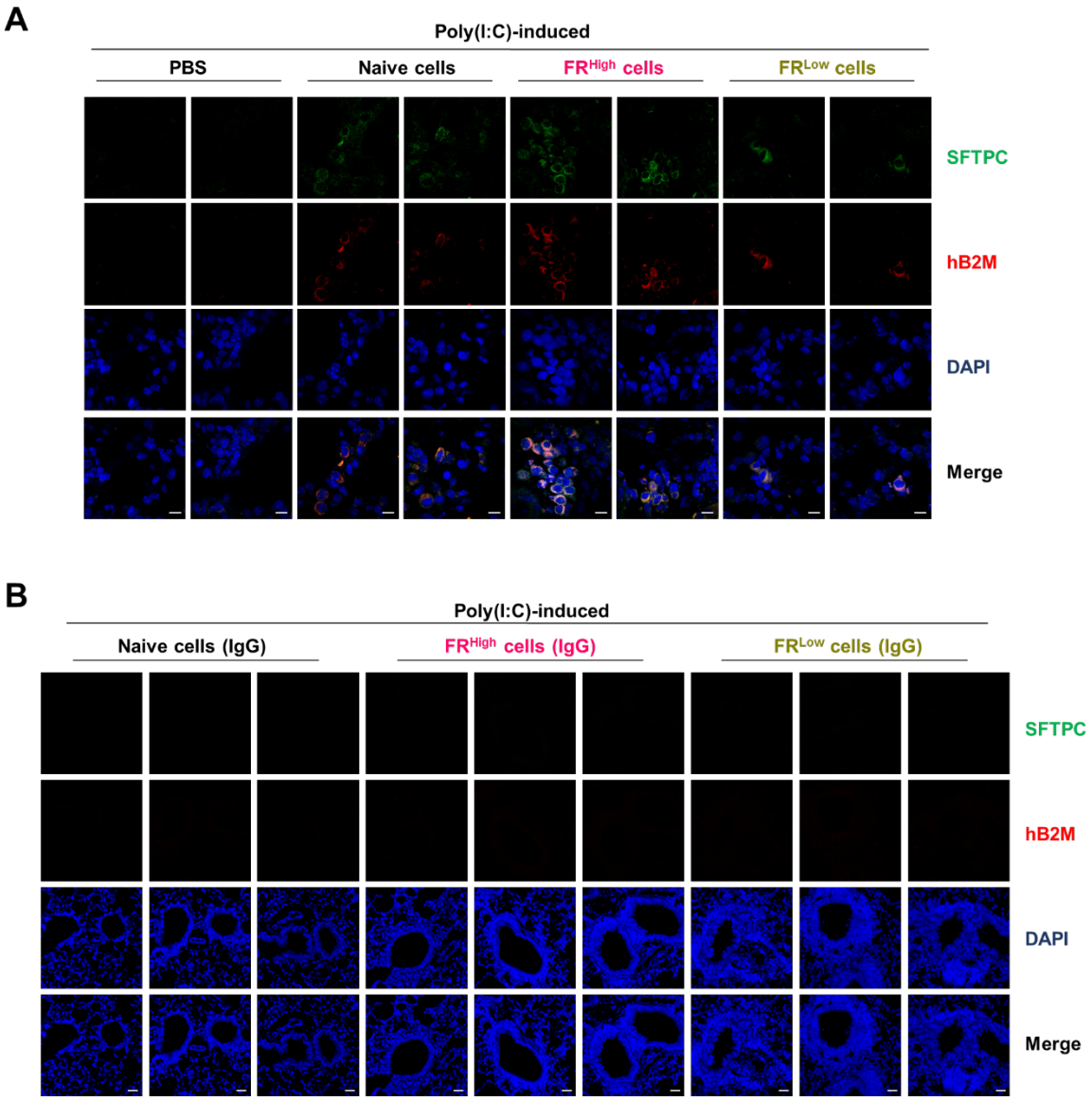

Figure S7. Immunostaining Analysis for Cellular Properties of Transplanted hES-MSCs, Related to Figure 7.

(A) Representative confocal images of lung tissue sections of poly(I:C)-induced asthma mice administrated with unsorted control (naive), FR^{High}, and FR^{Low} hES-MSCs or phosphate-buffered saline (PBS) after double staining for human β-2 microglobulin expressing cells (hB2M, red) and prosurfactant protein C (SFTPC, green) expressing type-2 alveolar cells. Nuclei were stained with DAPI (blue). (B) For negative control experiments, lung tissues of poly(I:C)-induced asthma animals administrated with the indicated hES-MSCs were co-stained with mouse and rabbit IgG control antibodies. Scale bar, 10 μm.

Table S1. K_D Values for Thiol Compounds Reacting with FreSHtracer
The K_D values of various thiols were determined as described in **Supplemental Experimental Procedures**.

Thiol compound	Structure	K_D (mM)
Glutathione	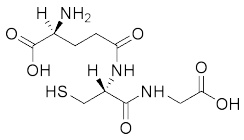	3.6 ± 0.3
Cysteine	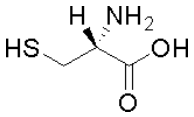	10.0 ± 0.7
Cysteamine	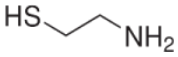	2.2 ± 0.4
β-mercaptoethanol	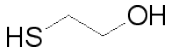	6.5 ± 0.5
Dithiothreitol	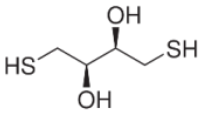	1.9 ± 0.2
N-acetyl cysteine	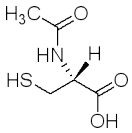	2.0 ± 0.4

Supplemental Experimental Procedures

Chemical synthesis of fluorescence probes

All of the chemicals used for probe synthesis were purchased from Sigma-Aldrich (St. Louis, MO) or TCI (Tokyo, Japan) and used without further purification. Dichloromethane was freshly dried via a solvent purification system (Glass Contour). Other solvents used were of anhydrous grade, obtained from Sigma-Aldrich or Acros (Geel, Belgium). Reactions requiring anhydrous conditions were performed under dry N_2. Silica gel (60 Å) was used for all column chromatography steps. Nuclear magnetic resonance (NMR) spectra were recorded at room temperature on Varian VNMRS400 or Mercury300 spectrometers. Chemical shifts are reported relative to the internal tetramethylsilane or residual solvent. Mass spectra were acquired at the National Center for Inter-University Research Facilities, Seoul National University. FreSHtracer was prepared according to our previously reported method (Cho and Choi, 2012). This probe is now commercially available (Cell2in, Seoul, Korea; http://www.cell2in.com).

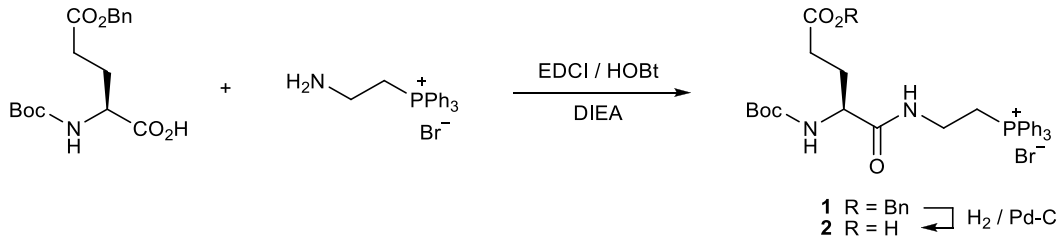

5-Benzyl *N*-(*tert*-butoxycarbonyl)-L-glutamate (0.10 g, 0.29 mmol), 1-hydroxybenzotriazole (HOBt, 80 mg, 2.0 eq.), and *N,N*-diisopropylethylamine (DIEA, 0.18 mL, 3.5 eq.) were dissolved in *N,N*-dimethylformamide (DMF, 1 mL). *N*-(3-dimethylaminopropyl)-*N'*-ethylcarbodiimide hydrochloride (EDCI, 0.11 g, 2.0 eq.) and (2-aminoethyl)-triphenylphosphonium bromide (Mari et al., 2013) (0.13 g, 1.2 eq.) were then added to the solution. After stirring for 16 h, the solution was diluted with ethyl acetate and then washed with 0.5 M citric acid, saturated $NaHCO_3$ aqueous solutions, and brine. The organic layer was dried over anhydrous Na_2SO_4 and concentrated under reduced pressure. The residue was purified by SiO_2 chromatography to obtain compound **1** as a white solid (0.16 g, 76%). ^{1}H NMR (400 MHz, $CDCl_3$): δ 9.49 (br s, 1H), 7.68–7.83 (m, 15H), 7.27–7.35 (m, 5H), 5.87 (d, J = 9.2 Hz, 1H), 5.08 (s, 2H), 4.18–4.23 (m, 1H), 3.61–3.87 (m, 4H), 2.43–2.47 (m, 2H), 2.12–2.22 (m, 1H), 1.94–2.01 (m, 1H), 1.43 (s, 9H); ^{13}C NMR (100 MHz, $CDCl_3$): δ 172.8, 172.7, 155.2, 135.8, 135.3 (d, $^4J_{CP}$ = 3.0 Hz), 133.4 (d, $^3J_{CP}$ = 10.4 Hz), 130.5 (d, $^2J_{CP}$ = 12.7 Hz), 128.4, 128.1, 128.0, 117.4 (d, $^1J_{CP}$ = 85.9 Hz), 79.2, 66.1, 53.9, 33.3, 30.4, 28.4, 28.3, 22.2 (d, $^1J_{CP}$ = 49.7 Hz); ^{31}P NMR (121 MHz, $CDCl_3$): δ 22.1; HRMS (*m/z*): $[M]^+$ calcd. for $C_{37}H_{42}N_2O_5P$, 625.2831; found. 625.2826.

Compound **1** (1.2 g, 1.7 mmol) was dissolved in the mixture of methanol (5 mL) and water (5 mL), and then 10 wt% Pd-C (0.12 g) was added to the solution. After stirring for 13 h under H_2 (1 atm), the reaction mixture was filtered through a Celite pad and the filtrate was concentrated under reduced pressure to give compound **2** as a white solid (1.04 g, 99%), which was used for the next reaction without further purification. ^{1}H NMR (400 MHz, $CDCl_3$): δ 8.95 (br s, 1H), 7.70–7.82 (m, 15H), 5.97 (br s, 1H), 4.16 (br s, 1H), 3.60–3.90 (m, 4H), 2.35–2.45 (m, 2H), 1.95–2.05 (m, 2H), 1.37 (s, 9H); ^{31}P NMR (121 MHz, $CDCl_3$): δ 22.1.

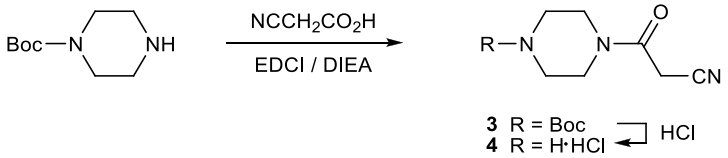

tert-Butyl pipeazine-1-carboxylate (1.0 g, 5.3 mmol) and cyanoacetic acid (0.54 g, 1.2 eq.) were dissolved in DMF (10 mL), and then DIEA (3.28 mL, 3.5 eq.) and EDCI (1.56 g, 1.5 eq.) were added to the solution. After stirring for 12 h, the solvent was evaporated under reduced pressure and the residue was purified by SiO_2 chromatography to give compound **3** as a white solid (1.13 g, 84%). ^{1}H NMR (400 MHz, $CDCl_3$): δ 3.60–3.64 (m, 2H), 3.50–3.55 (m, 2H), 3.51 (s, 2H), 3.43–3.48 (m, 4H), 1.47 (s, 9H); HRMS (*m/z*): $[M+H]^+$ calcd. for $C_{12}H_{20}N_3O_3$, 254.1505;

found. 254.1496.

Compound **3** (0.30 g, 1.2 mmol) was dissolved in a 4 M HCl dioxane solution (5 mL). After stirring for 1 h, the mixture was concentrated under reduced pressure to give compound **4** as a white solid in quantitative yield. This solid was used for the next reaction without further purification. ^{1}H NMR [400 MHz, dimethyl sulfoxide (DMSO)-d_6]: δ 9.54 (br s, 2H), 4.12 (s, 2H), 3.67–3.70 (m, 2H), 3.58–3.61 (m, 2H), 3.04–3.12 (m, 4H).

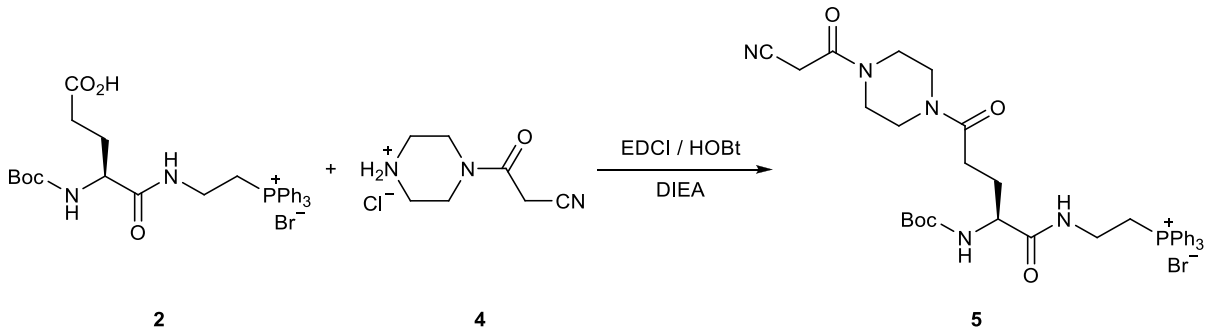

2 **4** **5**

Compound **2** (0.15 g, 0.24 mmol), compound **4** (49 mg, 1.05 eq.), and DIEA (0.15 mL, 3.5 eq.) were dissolved in DMF (2 mL), and then HOBt (3 mg, 0.1 eq.) and EDCI (95 mg, 2.0 eq.) were added to the solution. After stirring for 4 h, the solvent was evaporated under reduced pressure and the residue was purified by SiO_2 chromatography to give compound **5** as a yellowish-white solid (0.14 g, 78%). ^{1}H NMR (400 MHz, $CDCl_3$): δ (major conformer) 9.46 (br s 1H), 7.72–7.84 (m, 15H), 5.79 (d, J = 7.8 Hz, 1H), 4.15–4.21 (m, 1H), 3.47–3.79 (m, 14H), 2.50–2.60 (m, 2H), 2.12–2.15 (m, 1H), 2.00–2.04 (m, 1H), 1.42 (s, 9H); ^{13}C NMR (100 MHz, $CDCl_3$): δ (* major conformer; ** minor conformer) 172.8**, 172.7*, 171.2**, 171.0*, 161.1, 155.2, 135.3, 133.4 (d, $^3J_{CP}$ = 10.3 Hz), 130.5 (d, $^2J_{CP}$ = 12.7 Hz), 117.4 (d, $^1J_{CP}$ = 85.8 Hz), 114.5, 79.2, 54.0. 46.3*, 45.8**, 45.3*, 44.7**, 42.2**, 41.9*, 41.2**, 40.8*, 33.3, 30.0**, 29.5*, 29.2*, 28.9**, 28.3, 25.4, 22.2 (d, $^1J_{CP}$ = 49.8 Hz); ^{31}P NMR (121 MHz, $CDCl_3$): δ 22.1; HRMS (m/z): $[M]^+$ calcd. for $C_{37}H_{45}N_5O_5P$, 670.3158; found. 670.3157.

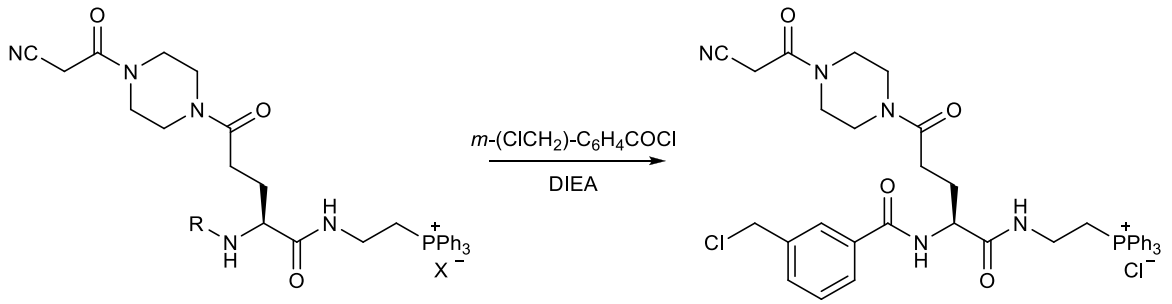

7

Compound **5** (0.23 g, 0.31 mmol) was dissolved in a 4 M HCl dioxane solution (3 mL). After stirring for 1 h, the mixture was concentrated under reduced pressure to give compound **6** as a yellowish-white solid in quantitative yield. This solid was used for the next reaction without further purification. ^{1}H NMR (400 MHz, DMSO-d_6): δ 9.44 (d, J = 6.1 Hz, 1H), 8.49 (br s, 3H), 7.76–7.94 (m, 15H), 4.09–4.11 (m, 1H), 3.80–3.84 (m, 2H), 3.33–3.50 (m, 12H), 2.50–2.55 (m, 2H), 1.94–1.98 (m, 2H); ^{31}P NMR (121 MHz, DMSO-d_6): δ 22.4.

Compound **6** (0.10 g, 0.15 mmol) and 3-(chloromethyl)benzoyl chloride (25 μL, 1.05 eq.) were dissolved in dichloromethane (1 mL), and DIEA (58 μL, 2.0 eq.) was added to the mixture. After stirring for 1 h, the solvent was evaporated under reduced pressure and the residue was purified by SiO_2 chromatography to give compound **7** as a white solid (0.10 g, 85%). ^{1}H NMR (400 MHz, $CDCl_3$): δ (major conformer) 9.65 (br s, 1H), 8.33 (d, J = 8.3 Hz, 1H), 8.13 (s, 1H), 8.05 (d, J = 7.8 Hz, 1H), 7.69–7.82 (m, 15H), 7.52 (d, J = 7.9 Hz, 1H), 7.42–7.46 (m, 1H), 4.74–4.79 (m, 1H), 4.65 (s, 2H), 3.35–3.74 (m, 14H), 2.53–2.60 (m, 2H), 2.25–2.30 (m, 2H); ^{13}C NMR (100

MHz, $CDCl_3$): δ ([*] major conformer; [**] minor conformer) 173.1[**], 173.0[*], 171.3[*], 171.2[**], 166.4, 160.9, 137.7, 135.5, 134.1, 133.5 (d, $^3J_{CP}$ = 10.3 Hz), 131.7, 130.6 (d, $^2J_{CP}$ = 12.7 Hz), 128.9, 128.3[*], 128.2[**], 127.8[*], 127.7[**], 117.5 (d, $^1J_{CP}$ = 85.9 Hz), 114.5, 54.2, 46.3[*], 45.9, 45.8[**], 45.3[*], 44.8[**], 42.1[**], 42.0[*], 41.3[**], 41.0[*], 30.2[**], 29.7[*], 28.3[*], 28.0[**], 25.3, 22.3 (d, $^1J_{CP}$ = 49.8 Hz); ^{31}P NMR (121 MHz, $CDCl_3$): δ 22.2; HRMS (*m/z*): $[M]^+$ calcd. for $C_{40}H_{42}ClN_5O_4P$, 722.2663; found. 722.2662.

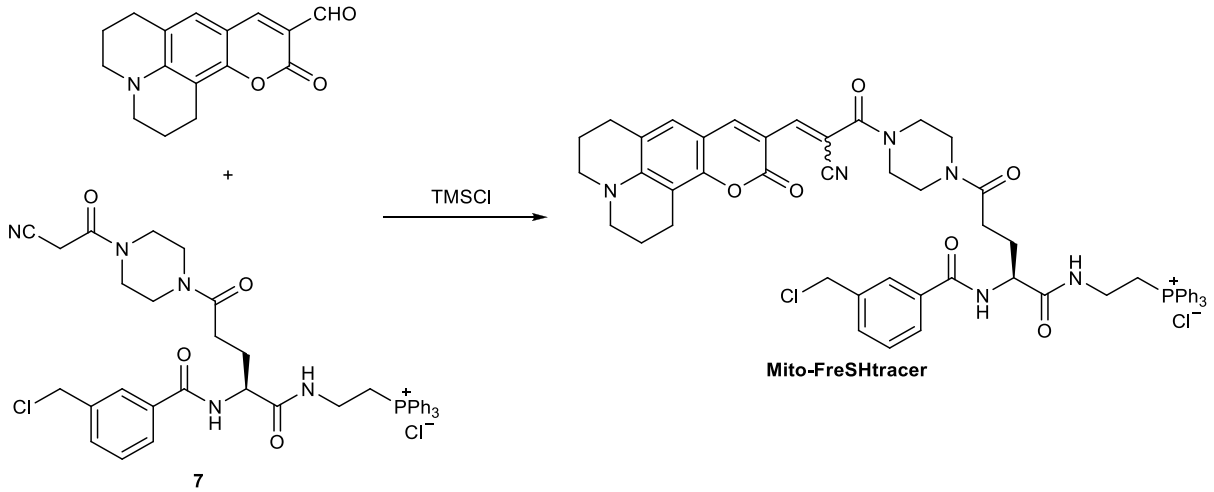

Compound **7** (0.12 g, 0.16 mmol) and 10-oxo-2,3,5,6-tetrahydro-1*H*,4*H*,10*H*-11-oxa-3a-azabenzo[*de*]anthracene-9-carbaldehyde (Yuan, 2011) (46 mg, 1.1 eq.) were dissolved in DMF (1 mL), and then chlorotrimethylsilane (60 μL, 3.0 eq.) was added to the solution (Ryabukhin S. V. , 2007). After stirring for 5 h at 130°C, the reaction mixture was concentrated under reduced pressure and the residue was purified by SiO_2 chromatography to give the final product as a red solid (79 mg, 50%). ^{1}H NMR (400 MHz, $CDCl_3$): δ (major isomer) 9.58 (br s, 1H), 8.63 (s, 1H), 8.40 (d, *J* = 7.4 Hz, 1H), 7.72–8.21 (m, 18H), 7.51 (d, *J* = 7.0 Hz, 1H), 7.42–7.45 (m, 1H), 7.00 (s, 1H), 4.74–4.80 (m, 1H), 4.60 (s, 2H), 3.58–3.73 (m, 12H), 3.33–3.38 (m, 4H), 2.83–2.87 (m, 2H), 2.72–2.78 (m, 2H), 2.55–2.58 (m, 2H), 2.27–2.31 (m, 2H), 1.97–2.04 (m, 4H); ^{13}C NMR (100 MHz, $CDCl_3$): δ (major isomer) 172.9, 171.1, 166.2, 163.9, 161.3, 152.5, 149.0, 145.9, 142.8, 137.6, 135.4, 134.0, 133.4 (d, $^3J_{CP}$ = 10.3 Hz), 131.6, 130.6 (d, $^2J_{CP}$ = 12.7 Hz), 128.8, 128.2, 127.7, 127.5, 119.9, 117.4 (d, $^1J_{CP}$ = 85.9 Hz), 117.1, 109.7, 108.2, 106.0, 100.4, 54.2, 50.4, 49.9, 45.9, 45.1 (br), 41.2 (br), 33.4, 29.9, 28.0, 27.2, 22.2 (d, $^1J_{CP}$ = 50.0 Hz), 20.9, 19.9, 19.8; ^{31}P NMR (121 MHz, $CDCl_3$): δ 22.2; HRMS (*m/z*): $[M]^+$ calcd. for $C_{56}H_{55}ClN_6O_6P$, 973.3609; found. 973.3616.

In vitro reactions of FreSHtracer with thiol compounds and reagents

Reactions between FreSHtracer and thiols were analyzed at room temperature with 10 μM FreSHtracer in a 10 mM phosphate buffer solution (PBS, pH 7.4) containing 150 mM NaCl and 2% (v/v) DMSO. The reaction was monitored by UV/Vis (Agilent 8453) and fluorescence (Hitachi F7000, or, Tecan Infinite 200Pro) spectroscopy. Fluorescence emissions were detected at 510 nm and 580 nm, exciting at 430 nm and 520 nm, respectively, to obtain the fluorescence ratio (FR; F_{510}/F_{580}). H_2O_2, glutathione (GSH), cysteine, cysteamine, N-acetylcysteine, ß-mercaptoethanol, dithiothreitol (DTT), diamide, buthionine sulfoximine (BSO), 3-(4,5-dimethylthiazolyl-2)-2,5-diphenyltetrazolium bromide (MTT), phorbol 12-myristate 13-acetate (PMA), NADPH, 1-chloro-2,4-dinitrobenzene (CDNB), and Ellman's reagent were purchased from Sigma-Aldrich. Yeast glutathione reductase was purchased from Calbiochem.

Calculation of the K_D values for thiol compounds

Mixtures of FreSHtracer (10 μM) with various concentrations of thiols were prepared in 10 mM PBS containing 150 mM NaCl and 2% (v/v) DMSO. To adjust the pH, acetate (4.0 and 5.0), CHES (9.0 and 10.0), or phosphate (other pH values) buffers were used. Fluorescence emission spectra were recorded 20 min after preparation of the mixtures. The emission intensities at 510 nm, over a range of thiol concentrations, were curve-fitted to an equation [1] describing the theoretical relation between the fluorescence intensity at equilibrium (F_{eq}) and the dissociation constant (K_D):

$$F_{eq} = k\{[\text{FreSH}]_T + [\text{thiol}]_T + K_D - \sqrt{([\text{FreSH}]_T + [\text{thiol}]_T + K_D)^2 - 4[\text{FreSH}]_T[\text{thiol}]_T}\} \quad [1]$$

In equation [1], $[\text{FreSH}]_T$ and $[\text{thiol}]_T$ denote the total concentrations of FreSHtracer and thiol, respectively.

Calculation of the rate constants for the reactions between FreSHtracer and thiols

FreSHtracer was added to GSH or protein solution in reaction buffer, and fluorescence emission (F_{510}) was detected at 510 nm with excitation at 430 nm. The kinetic experiments were performed using an initial FreSHtracer concentration of 10 μM. The data were analyzed using SigmaPlot 2000 (SPSS) and fitted to equation [2], which describes how the fluorescence intensities change as the reaction approaches equilibrium:

$$F(t) = F_0 + F_{eq}(1 - e^{(k_f[\text{thiol}]_T + k_r)t}) \quad [2]$$

In equation [2], F_0 and F_{eq} are the fluorescence intensities at the beginning of the reaction and at equilibrium, respectively; k_f and k_r are the rate constants for the forward and reverse reactions, respectively; and $[\text{thiol}]_T$ is the total concentration of either GSH or PSH. The reactive thiol concentrations of PSH solutions were measured by performing Ellman's assay. The reactions were performed at room temperature in 10 mM PBS (pH 7.4) containing 150 mM NaCl and 2% DMSO.

Preparation of protein solutions

HeLa cells were cultured for two days in a 150-mm dish. After reaching 80% confluence, the cells were harvested by scraping in PBS, followed by centrifugation. To prepare a protein solution, the cells were resuspended in PBS containing 0.1% Triton X-100 and completely disrupted by sonication. Following centrifugation at 12,000 × *g* for 10 min at 4°C, the lysates were dialyzed in cold PBS to remove low-molecular-weight thiol species, including GSH. The protein concentration was determined by the bicinchoninic acid method. These preparations were used as protein (PSH) solutions in further experiments.

In vitro measurement of GSH levels

To determine the GSH concentrations in BSO-treated HeLa cells, the cells were cultured in 96-well plates (White clear bottom, Corning) and then treated with BSO for 48 h. After washing twice with Hanks' buffered salt solution, the total GSH and GSSG concentrations were determined using a GSH/GSSG-Glo Assay kit (Promega). The concentration of reduced GSH was determined by subtracting the GSSG concentration from the total GSH concentration. Calculation of intracellular GSH concentrations in HeLa cells was based on an estimated average cell volume of 2600 μm^3 (Zhao et al., 2008) and total cell numbers.

MTT colorimetric assays

HeLa cells (5×10^3 cells/well), hBM-MSCs (1.3×10^3 cells/well), and hES-MSCs (1×10^4 cells/well) were cultured in 96-well dishes for 18 h and treated for 24 h with either DMSO or various concentrations of FreSHtracer. After washing with PBS, the cells were incubated for 3–4 h in MTT solution (500 μg/mL in culture medium). The MTT solution was removed, and DMSO was added to dissolve the formazan crystals. The 96-well dishes were incubated in the dark, and then the absorbance at 570 nm in each well was measured on a microplate spectrophotometer. Each treatment was performed in triplicate.

Stem cell culture and characterization in vitro and in vivo

hES-MSCs were grown in EGM2-MV medium (Lonza, Walkersville, MD) in tissue culture dishes coated with a type-I collagen from the rat tail (Sigma-Aldrich, St. Louis, MO; 150 μg per 100-pi dish), as previously described (Hong et al., 2015). hBM-MSCs (Lonza, Walkersville, MD) were cultured according to the manufacturer's instructions. The cells were loaded with 2 μM FreSHtracer for 2 h in culture medium and were subsequently sorted at 4°C according to their FR levels using an AriaIII Flow Cytometer System (BD Biosciences, San Jose, CA). FR^{High}, FR^{Mid}, and FR^{Low} fractions were collected and prepared for further analyses. The fluorescence intensities of cells were detected at Ex405-Em525/50 and Ex561-Em582/15. The sorted cells were washed twice with 50 mL PBS to remove the FreSHtracer from the cells and then further cultivated in culture medium for 24 h prior to conducting functional in vitro or in vivo experiments, as described below. Monitoring of intracellular FR changes following H_2O_2 treatment was achieved by confocal microscopy, as described in the main text. In vitro assays for cell proliferation, colony-forming unit-fibroblast (CFU-F), multipotency (in vitro differentiation into chondrogenic, adipogenic, or osteogenic lineages), and cell migration were performed as previously described (Kang et al., 2015). Chemotactic activity was measured using Boyden chambers with 8-μm pores (Corning, Corning, NY) in which 10 ng/mL platelet-derived growth factor (PDGF)-AA; R&D Systems, Minneapolis, MN) or 150 ng/mL stromal-derived factor 1-alpha (SDF1α; R&D Systems, Minneapolis, MN) was added to the lower chamber. To inhibit the PDGF signaling cascade, we used STI571 (Selleckchem, Houston, TX), a PDFGFR inhibitor. The stained cells on the lower side of the membranes were quantified by digital image analysis using Image Pro 5.0 software (Media-Cybernetics, Rockville, MD).

To evaluate the in vivo therapeutic potency of the sorted hES-MSCs, we generated a murine model of severe asthma as follows. Six-week-old BALB/c mice (OrientBio, Gapyong, Gyeonggi-do, Korea) were sensitized and challenged by intranasal administration with 75 μg ovalbumin (OVA; Sigma-Aldrich, St. Louis, MO) and 10 μg of polyI:C (Calbiochem, San Diego, CA) at days 0, 1, 2, 3, 7, 14, 21, 22, and 23. The mice were injected intravascularly with 3×10^5 hES-MSCs sorted according to the FR (as described above) on day 15. Histological examination and bronchoalveolar lavage fluid analysis were performed as previously described (Jin et al., 2016). The engraftment of the administrated hES-MSCs was determined by immunofluorescence analysis of human β2-microglobulin (primary mouse monoclonal antibody, Santa Cruz Biotechnology, Dallas, TX) and visualized using an Alexa546-labeled anti-mouse secondary antibody (Invitrogen, Carlsbad, CA). The differentiation lineage was evaluated by co-staining for human β2-microglobulin and prosurfactant protein C (rabbit polyclonal, Abcam, Cambridge, UK), as visualized with an Alexa488-labeled anti-mouse secondary antibody (Invitrogen, Carlsbad, CA). Nuclei were counterstained using 4′6-diamino-2-phenylinodole (DAPI; Sigma-Aldrich, St. Louis, MO). Stained samples were photographed on an inverted fluorescence microscope (EVOS FL Color Imaging System, Life Technologies) or Zeiss LSM780 AxioObserver.Z1 confocal microscope system (Carl Zeiss, Munich, Germany). All animal experiments were approved and performed in accordance with guidelines set by the Institutional Animal Care and Use Committee of the University of the Ulsan College of Medicine (2015-12-061).

Quantitative PCR

The primers for human and mouse transcripts were as follows.

Genes	Forward	Reverse
For human genes		
GAPDH	ACCCACTCCTCCACCTTTGA	TGTTGCTGTAGCCAAATTCGTT
OCT4	GAGCCCTGCACCGTCACC	TTGATGTCCTGGGACTCCTCC
SOX2	TACAGCATGTCCTACTCGCAGC	GAGGAAGAGGTAACCACAGGGG
CXCR4	ACTACACCGAGGAAATGGGCT	CCCACAATGCCAGTTAAGAAGA
cMET	AGCGTCAACAGAGGGACCT	GCAGTGAACCTCCGACTGTATG

PDGFRA	TTGAAGGCAGGCACATTTACA	GCGACAAGGTATAATGGCAGAAT
PDGFRB	TGATGCCGAGGAACTATTCATCT	TTTCTTCTCGTGCAGTGTCAC
VEGFR1	CTCTCTCCCTGATCGGTGACA	GGAGGGCAGAGCTGAGTGTTAG
VEGFR2	GGTTGCATTACTGTACCCATCATTT	TGAGATGGAATCTGACCATGTTG
ANGPT1	TGCTCACGTGGCTCGACTATA	AGCACAGCAAGCTCAGCAGTTT
CSF1	TGCTGGAGAAGGTCAAGAATGTC	GTTGTTGCAGTTCTTGCTGAAAA
IDO1	TCCGTGAGTTTGTCCTTTCAAA	CAGGGAGACCAGAGCTTTCACA
AP2	GGGTCACAGCACCCTCCTGA	GGTTTGGCCATGCCAGCCAC
ACAN	AGCCTGCGCTCCAATGACT	TAATGGAACACGATGCCTTTCA
SOX9	TTCCGCGACGTGGACAT	TCAAACTCGTTGACATCGAAGGT
RUNX2	TCTTAGAACAAATTCTGCCCTTT	TGCTTTGGTCTTGAAATCACA
OCN	AGCAAAGGTGCAGCCTTTGT	GCGCCTGGGTCTCTTCACT
ALP	GACCTCCTCGGAAGACACTC	TGAAGGGCTTCTTGTCTGTG
For mouse genes		
Gapdh	AGGTCGGTGTGAACGGATTTG	TGTAGACCATGTAGTTGAGGTCA
Oct4	GAAGCAGAAGAGGATCACCTTG	TTCTTAAGGCTGAGCTGCAAG
Sox2	GCTCGCAGACCTACATGAACG	GCCTCGGACTTGACCACAGA
Nanog	CTTTCACCTATTAAGGTGCTTGC	TGGCATCGGTTCATCATGGTAC
cMyc	TCTCCATCCTATGTTGCGGTC	TCCAAGTAACTCGGTCATCATCTC
Klf2	AGGCCTGTGGGTTCGCTATAA A	GGCAAATTATGGCTCAAAGTAGCAG
Klf4	CCATTATCAAGAGCTCATGCCA	GTTTTGCCACAGCCTGCATAG
Rex1	TCCATGGCATAGTTCCAACAG	TAACTGATTTTCTGCCGTATGC
Esrrb	TGGGCCTAGCAGGGTCAGA	TGCCACCTGTTTCTCATGAGTAG
Neurog2	TGTAAGGGTTGAATGCAAGCGTGG	GTGTGTGGCTGATCCTGGCAATGC
Olig2	GAGCACTGCACTTGACTTCTTTCC	AGGACCCTAAGTGCTTCTGATACC
T	GCTTCAAGGAGCTAACTAACGAG	CCAGCAAGAAAGAGTACATGG
Nkx2.5	CTTCAAGCAACAGCGGTACCT	CGCTGTCGCTTGCACTTGTA
Neurog1	GGTTTGGAAAAGGGACAGATGAGC	AAGCCTTGCCATTGTATTGTCAGC
Neurod1	AGGGGATCAAAGTTCCTGTTCACC	AGGTCACAGGTAGTAAAATGCTGG
Nkx2.2	GGAGCACAATCTGGTCATCTGTGG	CAGTTGACATCCACAAGGCAGACG
Ascl2	CCAAATGCCAAGTGCTGACTGACC	CAGAGGTCATCTTTATTGTGCTCC
Gfap	TGTACTAACAGAGCGAGCCTATGC	GGGACTTGCTGCCTTTAACATTGG
S100b	TGGACTTGAGGCTTTCTAACTTGC	ATGCGAAGGCATTGTTCAGTTGAC
Atoh	TGGGAGTTCATCCTTGCGTGTTGC	AGACACACTGCTGGACACACTTGG
Mlc2v	TCAGCTGCATTGACCAGAAC	CCCGAAGAGTGTGAGGAAGA
Runx1	GAGATTCAACGACCTCAGGTTT	TGTAAAGACGGTGATGGTCAGA
a-Actin	GTGTGACATCGATATCCGCAAA	GAAGCACTTGCGGTGGACAATG
cTnT	TGAAGAAGCCAAAGATGCTGAA	CACCAAGTTGGGCATGAAGAG
Tnfa	CCCTCACACTCAGATCATCTTCT	GCTACGACGTGGGCTACAG
Ccl2	GGCTCAGCCAGATGCAGTTAA	CCAGCCTACTCATTGGGATCA
Il1b	CTACAGGCTCCGAGATGAACAAC	GTCCATTGAGGTGGAGAGCTTTC
Il12a	GTGGCCATCGATGAGCTGAT	TCTGCTTCTCCCACAGGAGGTT
Il18	GACTCTTGCGTCAACTTCAAGG	CAGGCTGTCTTTTGTCAACGA

Reactions were performed with a KAPA SYBR FAST qPCR Kit (Kapa Biosystems) using a CFX96TM Real-Time system (Bio-Rad).

Western blotting

Cell lysates were prepared in lysis buffer (50 mM Tris, pH 7.5, 150 mM NaCl, 1 mM ethylenediaminetetraacetic acid, 1% Triton X-100, and a Roche protease inhibitor cocktail), resolved via sodium dodecyl sulfate-polyacrylamide gel electrophoresis, and transferred to a nitrocellulose membrane. The primary antibodies used were: Oct4 (SC5279, Santa Cruz Biotechnology, Dallas, TX), Nanog (RCAB001P, ReproCELL, Kanagawa, Japan), Sox2 (Ab92494, Abcam, Cambridge, UK), Klf4 (4038, Cell Signaling Technology, Danvers, MA), and β-

actin (A5441, Sigma-Aldrich, St. Louis, MO). The secondary antibody was goat anti-rabbit IgG-HRP (sc-2004) or goat anti-mouse IgG-HRP (sc-2005), both from Santa Cruz Biotechnology (Dallas, TX).

Supplemental References

Cho, A.Y., and Choi, K. (2012). A coumarin-based fluorescence sensor for the reversible detection of thiols. Chem Lett *41*, 1611-1612.

Filonov, G.S., Piatkevich, K.D., Ting, L.M., Zhang, J., Kim, K., and Verkhusha, V.V. (2011). Bright and stable near-infrared fluorescent protein for in vivo imaging. Nat Biotechnol *29*, 757-761.

Hong, K.S., Bae, D., Choi, Y., Kang, S.W., Moon, S.H., Lee, H.T., and Chung, H.M. (2015). A porous membrane-mediated isolation of mesenchymal stem cells from human embryonic stem cells. Tissue Eng Part C Methods *21*, 322-329.

Jin, H.J., Lee, H.J., Heo, J., Lim, J., Kim, M., Kim, M.K., Nam, H.Y., Hong, G.H., Cho, Y.S., Choi, S.J.*, et al.* (2016). Senescence-associated MCP-1 secretion is dependent on a decline in BMI1 in human mesenchymal stromal cells. Antioxid Redox Signal *24*, 471-485.

Kang, H., Kim, K.H., Lim, J., Kim, Y.S., Heo, J., Choi, J., Jeong, J., Kim, Y., Kim, S.W., Oh, Y.M.*, et al.* (2015). The therapeutic effects of human mesenchymal stem cells primed with sphingosine-1 phosphate on pulmonary artery hypertension. Stem Cells Dev *24*, 1658-1671.

Mari, M., Morales, A., Colell, A., Garcia-Ruiz, C., Kaplowitz, N., and Fernandez-Checa, J.C. (2013). Mitochondrial glutathione: features, regulation and role in disease. Biochim Biophys Acta *1830*, 3317-3328.

Ryabukhin S. V. , P.A.S., Volochnyuk D. M. , Pipko S. E., Shivanyuk A. N., and Tolmachev A. A. (2007). Combinatorial Knoevenagel reactions. J Comb Chem *9*, 1073–1078.

Yuan, L., Lin, W. Y., Song, J. Z. & Yang, Y. T. (2011). Development of an ICT-based ratiometric fluorescent hypochlorite probe suitable for living cell imaging. Chem Commun *47*, 12691–12693.

Zhao, L., Kroenke, C.D., Song, J., Piwnica-Worms, D., Ackerman, J.J., and Neil, J.J. (2008). Intracellular water-specific MR of microbead-adherent cells: the HeLa cell intracellular water exchange lifetime. NMR Biomed *21*, 159-164.